Astronomy & Astrophysics manuscript no. n6253
April 22, 2010

VLT multi-epoch radial velocity survey toward NGC 6253 ⋆

Analysis of three transiting planetary candidates

M. Montalto[2,1], S. Villanova[3], J. Koppenhoefer[1,2]

[1] Universitaets-Sternwarte der Ludwig-Maximilians-Universitaet, Scheinerstr.1, 81679 Muenchen, Germany.
[2] Max-Planck-Institute for Extraterrestrial Physics, Giessenbachstr., Garching b Muenchen, 85741, Germany.
[3] Grupo de Astronomia, Departamento de Fisica, Casilla 160, Universidad de Conception, Chile

ABSTRACT

Context.
Aims. We measured the radial velocity of 139 stars in the region of NGC 6253, discussing cluster's membership and binarity in this sample, complementing our analysis with photometric, proper motion, and radial velocity data available from previous studies of this cluster, and analyzing three planetary transiting candidates we found in the field of NGC 6253.
Methods. Spectra were obtained with the UVES and GIRAFFE spectrographs at the VLT, during three epochs in August 2008.
Results. The mean radial velocity of the cluster is $(\overline{RV_{cl}} \pm \overline{\sigma_{cl}}) = (-29.11 \pm 0.85)$ km/s. Using both radial velocities and proper motions we found 35 cluster's members, among which 12 are likely cluster's close binary systems. One star may have a sub-stellar companion, requiring a more intensive follow-up. Our results are in good agreement with past radial velocity and photometric measurements. Furthermore, using our photometry, astrometry and spectroscopy we identified a new sub-giant branch eclipsing binary system, member of the cluster. The cluster's close binary frequency at (29±9)% (34%±10% once including long period binaries), appears higher than the field binary frequency equal to (22±5)%, though these estimates are still consistent within the uncertainties. Among the three transiting planetary candidates the brightest one ($V = 15.26$) is worth to be more intensively investigated with higher percision spectroscopy.
Conclusions. We discussed the possibility to detect sub-stellar companions (brown dwarfs and planets) with the radial velocity technique (both with UVES/GIRAFFE and HARPS) around turn-off stars of old open clusters. We isolated 5 stars that are optimal targets to search for planetary mass companions with HARPS. Our optimized strategy minimizes the observing time requested to isolate and follow-up best planetary candidates in clusters with high precision spectrographs, an important aspect given the faintness of the target stars.

Key words. Galaxy:Open Clusters and Associations:individual:NGC 6253–stars:radial velocities

1. Introduction

The advent of multi-object spectrographs feeding large aperture telescopes offers the possibility to obtain simultaneous, repeated, and accurate spectroscopic measurements of a large sample of stars. The application of this technique to the study of open clusters is of particular interest. While open clusters photometric surveys are now routinely performed spanning typically several consecutive nights, there are relatively few multi-epoch radial velocity surveys targeting these objects (Mermilliod et al. 2009; Hole et al. 2009). Besides allowing further culling of cluster's members, multiple radial velocity measurements allow a more complete census of binary and multiple systems. Spectroscopic follow-up of eclipsing binary systems that belong to open clusters gives the opportunity to derive accurate stellar masses, constraining models of stellar evolution (e. g. Southworth & Clausen 2006). Moreover, the increasing stability and accuracy of modern spectrographs is driving toward detection of binary systems with low mass companions (such as brown dwarfs and planets) also in open clusters, where target stars are typically fainter than those observed in common radial velocity planet searches in the solar surrounding.

In this work, we focused our attention on the old and metal-rich open cluster NGC 6253 ($\alpha_{2000} = 16^h\,59^m\,05^s, \delta_{2000} = -52^\circ\,42'\,30''$, $l = 335.^\circ5, b = -6.^\circ3$). This cluster was selected as part of our project aimed at searching for transiting hot-jupiter planets in metal-rich open clusters (Montalto et al. 2007). In 2004, we performed a photometric transit search toward NGC 6253 using the WFI at the 2.2m Telescope for ten consecutive nights (Montalto et al. 2009), identifying three transiting planet candidates.

In the solar neighborhood, FGK metal-rich dwarf stars have higher probability to host jupiter-like planets (Gonzalez 1998, Santos et al. 2001, Fischer & Valenti 2005). Accordingly to the most accredited explanation that the planet-metallicity correlation is of primordial origin, we expect a higher planet discovery rate targeting preferentially stars borned in metal-rich environments. While at solar metallicity the frequency of planets (with period P < 4 years, and radial velocity semi-amplitude $K > 30$ m/s) around FGK dwarf stars in the solar neighbourhood is about 3%, at the metallicity of NGC 6253, the expected frequency is around 18%, as can be deduced from Fischer & Valenti (2005).

Send offprint requests to: M. Montalto,
e-mail: montalto@usm.uni-muenchen.de

⋆ Based on observations collected at the European Organization for Astronomical Research in the Southern Hemisphere (ESO) in Paranal during program 381.C-0270(A), and in La Silla during program 073.C-0227(A), and program 083.A-9001(C) thanks to Max Planck Institute for Extraterrestrial Physics reserved time.

Since the large expected frequency of planets in metal rich clusters, these objects are top targets for planet searches and offer an excellent natural laboratory to test ideas of planet formation and evolution, while probing at the same time the effects of the environment.

Searches for planets around dwarf stars in clusters have not yet provided even bona-fide planetary candidates. This result may still be due to statistical problems, since in particular open clusters are tipically loosely populated and the most widely used technique to detect planets in such environments is the transit method. However, the increasingly larger number of surveys and the lack of detections could start to reveal some fundamental differences between planet formation processes around field and cluster's dwarf stars. It is then of primary importance to continue monitoring clusters and estabilish on a firmly observational basis if there is indeed a difference between the planet frequency in these environments and in the field.

In this work we present some preliminary results regarding our survey toward NGC 6253. In August 2008, we followed-up with VLT three candidate transiting planets we found in the region of this cluster. We will dedicate a forthcoming contribution to the study of planet frequency in the field and in the cluster. Our observational strategy was tied also to the study of cluster's members and surrounding field stars, and here we present the results of the complete multi-epoch radial velocity campaign toward NGC 6253. We used FLAMES in MEDUSA mode, targeting a total of 204 stars in the region of the cluster.

In this work we then explore the possibility to search for planetary companions around dwarf stars of old open clusters by means of the radial velocity technique. This detection method would greatly increase our chances to detect planetary mass companions, allowing us to overcome the problem of the small sample of stars available in clusters. However such technique has been applyied systematically only to the Hyades cluster so far (Cochran et al. 2002, Paulson et al. 2002, Paulson et al. 2003) given the closeness and consequently brightness of its members. In young clusters planet detection is significantly hampered and complicated by stellar activity (Paulson et al. 2004a, Paulson et al. 2004b). Old open clusters should be better targets, although the faintness of their members seems to significantly limit the application of the radial velocity technique, requiring in general a very large investment of observing time. Here we discuss an optimized observing strategy aimed at isolating only the most promising objects to follow-up with high precision spectroscopy, involving the use of photometry, astrometry and multi-object spectroscopy. Beside resulting in a great improvement in the knowledge of cluster's properties this method minimizes the time needed to identify and follow-up best candidates. The application of this technique to the particular case of NGC 6253 is of special interest given the characteristics of this cluster.

NGC 6253 has been studied by several authors in the past, both photometrically (Bragaglia et al. 1997, Piatti et al. 1998, Sagar, Munari, & de Boer 2001, Twarog, Anthony-Twarog & De Lee 2003, Anthony-Twarog, Twarog, & Mayer 2007, Montalto et al. 2009, De Marchi et al. 2009), and spectroscopically (Carretta et al. 2000, Carretta, Bragaglia & Gratton 2007, Sestito et al. 2007). In addition, in Montalto et al. (2009) we calculated proper motion membership probabilities.

These studies have demonstrated that NGC 6253 is an old (∼3.5 Gyr, e. g. Montalto et al. 2009), and metal-rich cluster ([Fe/H]=+0.39±0.07 Sestito et al. 2007; [Fe/H]=+0.46 Carretta, Bragaglia & Gratton 2007), being in fact one of the most metal-rich open clusters of the Galaxy. It is also one of the few old open clusters located inward the solar ring (Carraro et al. 2005a, 2005b), at a Galactocentric distance of around 6 kpc, where more prohibitive environmental conditions in general prevent clusters' survival (Wielen 1971). NGC 6253 it is also important in the more general context of stellar population studies, offering an homogeneous sample of coeval metal-rich stars against which stellar models at this extreme metallicity can be tested and compared. Its peculiar location in the Galactic disk gives the opportunity to extend toward the inner regions of the Galaxy the baseline for the study of the Galactic disk radial abundance, which is a basic ingredient of Galactic chemical evolution models (Tosi 1996).

This paper is organized as follows: in Sect. 2, we describe our observations; in Sect. 3, we give a detailed description of reductions and calibrations; in Sect. 4, we discuss cluster's membership and binarity in our sample; in Sect. 5, we analyze our three transiting planetary candidates; in Sect. 6, we focus our attention on four detached eclipsing binary systems; in Sect. 7, we discuss a new eclipsing binary system located at the sub-giant branch of NGC 6253; in Sect. 8, we present an optimized strategy to search for sub-stellar objects with the radial velocity technique around turn-off stars of old open clusters; in Sect. 9, we discuss a method to constrain the minimum mass and period of cluster's close binary systems, detected by RV surveys; finally in Sect. 10, we summarize and conclude.

2. Observations

The observations were obtained using the FLAMES facility (Pasquini et al. 2002) at the UT2 (Kueyen telescope), in Paranal, Chile. FLAMES is the multi-object, intermediate and high resolution spectrograph of the VLT. It can access targets over a 25 arcmin diameter field of view, and it feeds two different spectrographs: UVES and GIRAFFE. While UVES provides the maximum resolution (R=47000), but can access up to 8 targets at the time, GIRAFFE has an intermediate resolution (either R≃25000 or R≃10000), allowing to target up to 130 objects at the time or to do integral field spectroscopy.

As reported in the previous section, our main purpose was to follow-up three planetary transiting candidates we found in the field of NGC 6253. Then, we used UVES in fiber mode, with the standard setup centered at 580nm. To maximize the scientific output of our research, we used simultaneously UVES with GIRAFFE, with the high resolution grating HR9B, covering 21.3nm centered at 525.8nm with a resolution R=25000.

Given the spatial distribution of the transiting candidates we decided to prepare two different configurations named NGC6253_A and NGC6253_B[1].

In each configuration the 8 fibers of UVES were allocated in the following manner: one fiber was dedicated to the simultaneous calibration, two fibers were allocated to two transiting candidate host stars, four (three in the second configuration) fibers to some known cluster's member stars, and one (two in the second configuration) to the sky. Since our faintest candidate planet host star ($V = 18.247$) was located in between the other two, we were able to observe it in both configurations in order to improve the S/N.

The GIRAFFE fibers were used to target other cluster's members, known photometric variables (De Marchi et al. 2009), allocated to the sky or simultaneous calibration lamps.

[1] This is also the nomenclature adopted for the data stored in the ESO archive, where we further distinguished the different observing nights, e.g. for the first configuration and the first night we used NGC6253_A_N1.

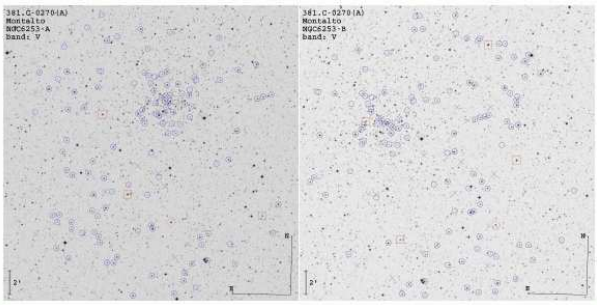

Fig. 1. The two UVES/MEDUSA configurations reported in the text. Circles denote the positions of the UVES/GIRAFFE targets. The rhombus corresponds to the VLT guide star, and the boxes to the three reference stars used by the Field Acquisition Coherent Bundle (FACB) guide fibers.

Table 1. Journal of observations.

Plate name	Date	MJD
NGC6253_A_N1	2008-08-17	54695.04805166
NGC6253_B_N1	2008-08-17	54695.01926262
NGC6253_A_N2	2008-08-20	54698.99723017
NGC6253_B_N2	2008-08-21	54699.02557366
NGC6253_A_N3	2008-08-25	54703.00230984
NGC6253_B_N3	2008-08-25	54703.03139454

The data were obtained during three nights between August 17, 2008 and August 25, 2008. The exposure time for each configuration was 1875 sec (15 min overhead), for a total observing time of ∼6 hours. The observations were performed in service mode. Table 1 provides a summary of our data.

We targeted a total of 204 stars, 44 of which present in both configurations. For a given star, we used always the same fiber (apart from the stars in common to the two configurations) to minimize systematic effects. We measured the radial velocity for a total of 139 stars. We were not able to obtain accurate radial velocities for 65 stars.

For 24 objects this was probably due to their faint magnitude, since they had $R > 16$. For the remaining 41 stars, either to their intrinsic characteristics (hot temperature, high rotation velocities, etc.) or bad fiber positioning, or blends.

Among the stars analyzed, 106 have 3 measurements (present only in one configuration), and 33 have 6 measurements (present in both configurations). We selected preferentially probable cluster's members, on the basis of colors, magnitudes and proper motion membership probabilities (MP). These probabilities were calculated in Montalto et al. (2009), considering likely cluster's members those stars located within a rectangle region of dimesion 6.3 x 7.9 arcmin inclusive of the cluster's center (see Montalto et al. 2009 for details), with magnitude $V < 18$, and that have MP>90% at $V = 12.5$, down to MP>50% at $V = 18$. The selected stars are representative of different stellar evolutionary stages, and include a sample of turn-off, sub-giant branch, red-giant branch, red-clump, and blue straggler stars. We also considered in our target list 16 stars present in the sample of variable stars compiled by De Marchi et al. (2009). These are: the contact binary (EW) 30341; the RS Canum Venaticorum variable (RS CVn) 44079; the detached binary systems (EA) 31195, 24487, 38138, 126376; the rotational variables (RO1, RO2, see De Marchi et al. 2009 for details) 9832, 6430; the long period variables 173273, 15343_2, 40819, 16649, 50025, 4306; the RR Lyrae (RR) 74452, and the δ Scuti (DSCT) 8420_6. One of these stars, the RS Canum Venaticorum variable (RS CVn) 44079, is a likely cluster's member. Finally, seven stars in the spectroscopic sample of Carretta et al. (2007) and Sestito et al (2007) were included in our list, further improving our chances to detect binarity for these objects. They are: stars 45410, 45412, 45413, and 45414 from Carretta et al. (2007), and stars 45404, 45421, 45474 from Sestito et al. (2007), all likely members of NGC 6253. The numeration of these stars is that one presented in the catalog of Montalto et al. (2009) or in De Marchi et al. (2010). The remaining stars in our list were selected considering either the need to have a sample of field objects against which comparing the results obtained for cluster's stars, or technical constraints like that the need to avoid putting the fiber buttons too close to each others.

3. Data reduction, and radial velocity measurement.

Data were reduced using the UVES and GIRAFFE pipelines (Ballester et al. 2000, Blecha et al. 2000) where raw data were bias-subtracted, flat-field corrected, extracted using the average extraction method, and wavelength-calibrated. GIRAFFE spectra were wavelength-calibrated using both prior and simultaneous calibration-lamp spectra, which assure a final systematic error in radial velocities lower than 100 m/s (Sommariva et al. 2009).

In particular, for each plate the wavelength calibration was firstly done using the next morning ThAr frame. Then a drift correction measured by the 5 simutaneous calibration lamps was applied. The drift was of the order of few hundred m/s

Finally, sky subtraction was applied. For what concerns UVES data, echelle orders were flux-calibrated using the master response curve of the instrument. Finally, the orders were merged to obtain a 1D spectrum. Radial velocities were obtained from the IRAF fxcor cross-correlation subroutine. Stellar spectra were cross-correlated with synthetic templates calculated by SPECTRUM[2]. The selection of a proper template for each star was mandatory because the targets have different spectral types and rotational velocities. For this reason we used 3 templates: the first calculated for the sun and valid for stars with effective temperatures in the range T_{eff} =4000-6500 K; the second calculated for T_{eff}=3500 K, which includes the strong molecular bands, and is valid for the coolest stars in our sample; the last calculated for T_{eff}=7000 K, valid for the hottest stars in our sample. In addition, the template for hot stars was divided in 7 sub-templates, calculated for rotational velocities equal to 0, 25, 50, 75, 100, 200, and 300 km/s. For each star we carefully compared the observed spectrum with our templates and, according to the visible spectral lines and to a rough estimation of the rotation, we chose the most appropriate one.

We calculated for each star the mean radial velocity ($\overline{RV_{obs}}$), and the dispersion ($\sigma_{\rm obs}$):

$$\overline{RV_{obs}} = \sum_i \frac{RV_i}{N} \quad (1)$$

$$\sigma_{obs} = \sqrt{\sum_i \frac{(RV_i - \overline{RV_{obs}})^2}{(N-1)}} \quad (2)$$

where RV_i is the i-th radial velocity measurement, and N is the total number of measurements for each star.

[2] See http://www.phys.appstate.edu/spectrum/spectrum.html for more details.

To determine the threshold for binary detection, we subdivided the stars in seven magnitude bins 0.5 mag wide between $11 < R < 14.5$, plus an additional large magnitude bin between $14 \leq R < 18$ (to account for the fewer number of stars in this magnitude range). We calculated the mean dispersion in each magnitude bin excluding stars with $\sigma_{obs} > 1$ km/s ($\sigma_{obs} > 2$ km/s, in the fainter large bin), applied a σ-clipping algorithm excluding all stars above $3.5 \times \sigma$ from the mean, and calculated the final value of the mean dispersions. We then performed a linear least square fit of the resulting values separating the brighter bins from the fainter one. Our result for the best-fit mean dispersion of *constant* stars ($\overline{\sigma_{\rm obs}}$) is given by the following equations:

$$\overline{\sigma_{obs}} = 0.030\,R - 0.130 \quad R < 14.5 \tag{3}$$

$$\overline{\sigma_{obs}} = 0.394\,R - 5.407 \quad R \geq 14.5 \tag{4}$$

We adopted a conservative threshold for binary detection given that only stars having $\sigma_{\rm obs} > 5 \times \overline{\sigma_{\rm obs}}$ were considered candidate spectroscopic binaries. In Fig. 2, we show the mean dispersion as a continuous line, and the $3 \times \overline{\sigma_{obs}}$, $5 \times \overline{\sigma_{obs}}$ as dotted and dashed lines respectively.

Throughout this paper we will call radial velocity variables simply *candidate close binary systems*, or *close binary systems*, though it is clear that they could also be multiple systems, or that the radial velocity variations may have other physical explanations. In particular, we used the adjective *close*, because our observations span a period of only eight days, and even when the binarity is inferred by means of a comparison with past literature results, those observations are separated at most by eight years with respect to our observations [3].

In Table 2 and in Table 3, we present the measured radial velocities for the analyzed objects, distinguishing between stars which are likely to be proper motion cluster's members (Table 2), and stars that are proper motion non members, or with doubtful/absent proper motions (Table 3).

4. Results

4.1. Cluster's mean radial velocity

The recession radial velocity of the cluster was calculated considering only proper motion cluster's members. Moreover, we excluded stars which are likely close binaries (see the previous section). Then we calculated the mean radial velocities ($\overline{RV_{obs}}$) of all the remaining stars, and used them to derive the cluster's mean radial velocity ($\overline{RV_{obs}}$), after applying an iterative 3-σ clipping algorithm, to exclude also long period binaries or residual contaminants. The resulting mean radial velocity of the cluster obtained after this procedure is $\overline{RV_{cl}} \pm \overline{\sigma_{cl}} = (-29.11 \pm 0.85)$ km/s, where the error is the error of the mean, and the root mean square of the residuals is $\sigma_{cl} = 4.26$ km/s, obtained from the remaining sample of 25 stars.

The cluster's velocity dispersion seems quite high, since typical values for open clusters of similar richness are around 1-2 km/s. This might indicate that there are still long-period binaries inflating the RV distribution. In Fig. 3, we present the radial velocity histogram for the 25 stars used above to calculate the cluster's mean radial velocity (upper panel), and for all the remaining objects (bottom panel), in bins of 4 km/s. Among the stars not considered in our calculation there are other very likely members, which will be discussed in the next Section.

[3] This is the case of the observations presented in Carretta et al. (2007). Sestito et al. (2007) measurements were obtained four years before us.

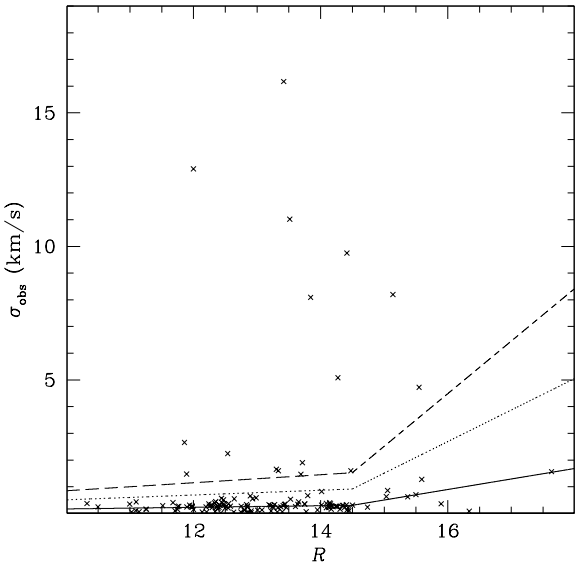

Fig. 2. Observed radial velocity dispersions ($\sigma_{\rm obs}$) against R-band magnitude. The continuous line indicates our best-fit for the typical dispersion ($\overline{\sigma_{obs}}$) of radial velocity *constant* stars. The dotted and dashed lines are the $3 \times \overline{\sigma_{obs}}$, and the $5 \times \overline{\sigma_{obs}}$ thresholds.

Considering only stars with radial velocities within 1-σ from the mean, the result is $\overline{RV_{cl}} \pm \overline{\sigma_{cl}} = (-28.98 \pm 0.12)$ km/s, and the scatter $\sigma_{cl} = 0.4$ km/s, calculated from a sample of 10 stars. These estimates are in reasonable agreement with previous literature results. Sestito et al. (2007), obtained a mean radial velocity equal to (-29.71±0.79) km/s from a sample of 4 stars. Carretta et al. (2007), obtained (-28.26±0.29) km/s from a sample of 4 stars.

4.2. Proper motion and radial velocity members

Among the sample of proper motion cluster's members, stars that have mean radial velocities ($\overline{RV_{obs}}$) satisfying the condition:

$$\left|\overline{RV_{obs}} - \overline{RV_{cl}}\right| < 3\,\sigma_{cl}, \tag{5}$$

were considered also radial velocity members. In Fig. 4, we present the $(R, B-R)$ color magnitude diagram for proper motion selected cluster's members (small black points), where stars having also radial velocity measurements are enlighted by colored squares. Moreover, stars that are likely close binaries (as obtained from our multi-epoch radial velocities), are framed in black squares. We overplot to the figure the best-fit isochrone taken from the Padova database (age=3.5 Gyr, Z=0.03, continuous line), and also the equal mass binary sequence (dashed line). The red squares represent stars that met both our proper motion, and radial velocity membership criteria. They are in total 30 stars. As shown in Fig. 4, these stars populate the turn-off, subgiant, red-giant branch, red-clump and blue straggler regions of the cluster, and are considered secure cluster members. Among them, the following objects are particularly interesting:

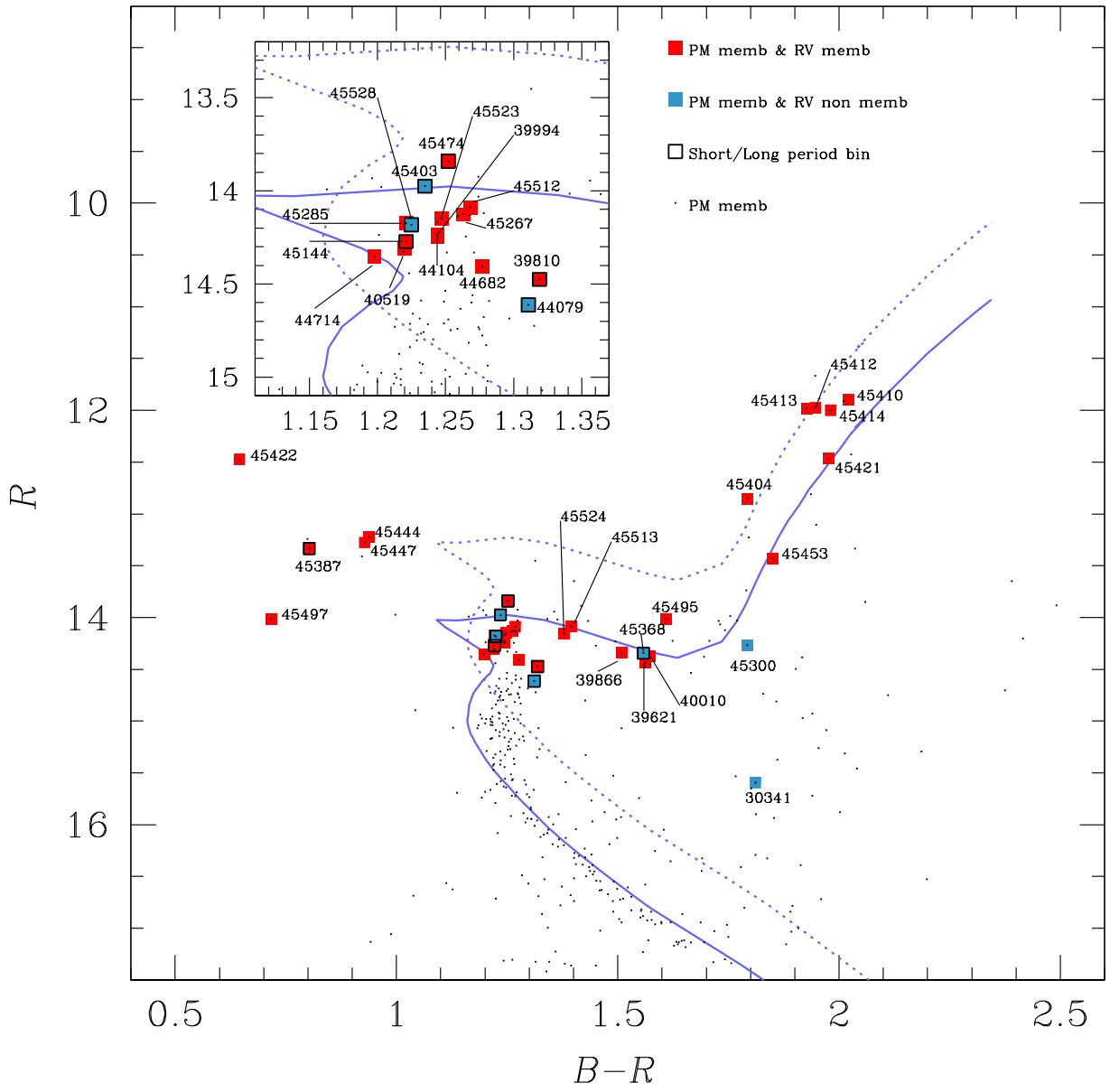

Fig. 4. *R*-band magnitude, and $B-R$ color, for proper motion selected members (small black points). Red squares indicate stars that are also radial velocity members, steel blue squares stars that appear radial velocity non members, and black framed squares stars that are likely close binary systems.

4.3. Star 39810

Star 39810 has a high proper motion membership probability (MP=95%), its mean radial velocity agrees with that one of the cluster ($\overline{RV_{obs}}$-$\overline{RV_{cl}}$ =0.037σ_{cl} = 0.159km/s), and it is located in the turn-off region of the cluster. Since from our repeated radial velocities we measured a dispersion σ_{obs} =1.595 km/s, ($\sigma_{obs}/\overline{\sigma_{obs}}$ = 5.242), we conclude that this object is also a candidate cluster's close binary system. This object is discussed in more detail in Sect. 9.

4.4. Star 45387

Star 45387 is a proper motion and radial velocity cluster's member (MP=97%, $\overline{RV_{obs}}$-$\overline{RV_{cl}}$ =0.115σ_{cl} = 0.492 km/s) located in the blue straggler region, and a likely close binary system (σ_{obs} = 1.602 km/s, $\sigma_{obs}/\overline{\sigma_{obs}}$ = 5.932).

4.5. Star 45144

Star 45144 is a proper motion and radial velocity cluster's member (MP=97%, $\overline{RV_{obs}}$-$\overline{RV_{cl}}$ =1.380σ_{cl} = 5.879 km/s) in the turn-off region. It is a likely close binary system (σ_{obs} = 5.081 km/s, $\sigma_{obs}/\overline{\sigma_{obs}}$ = 17.041).

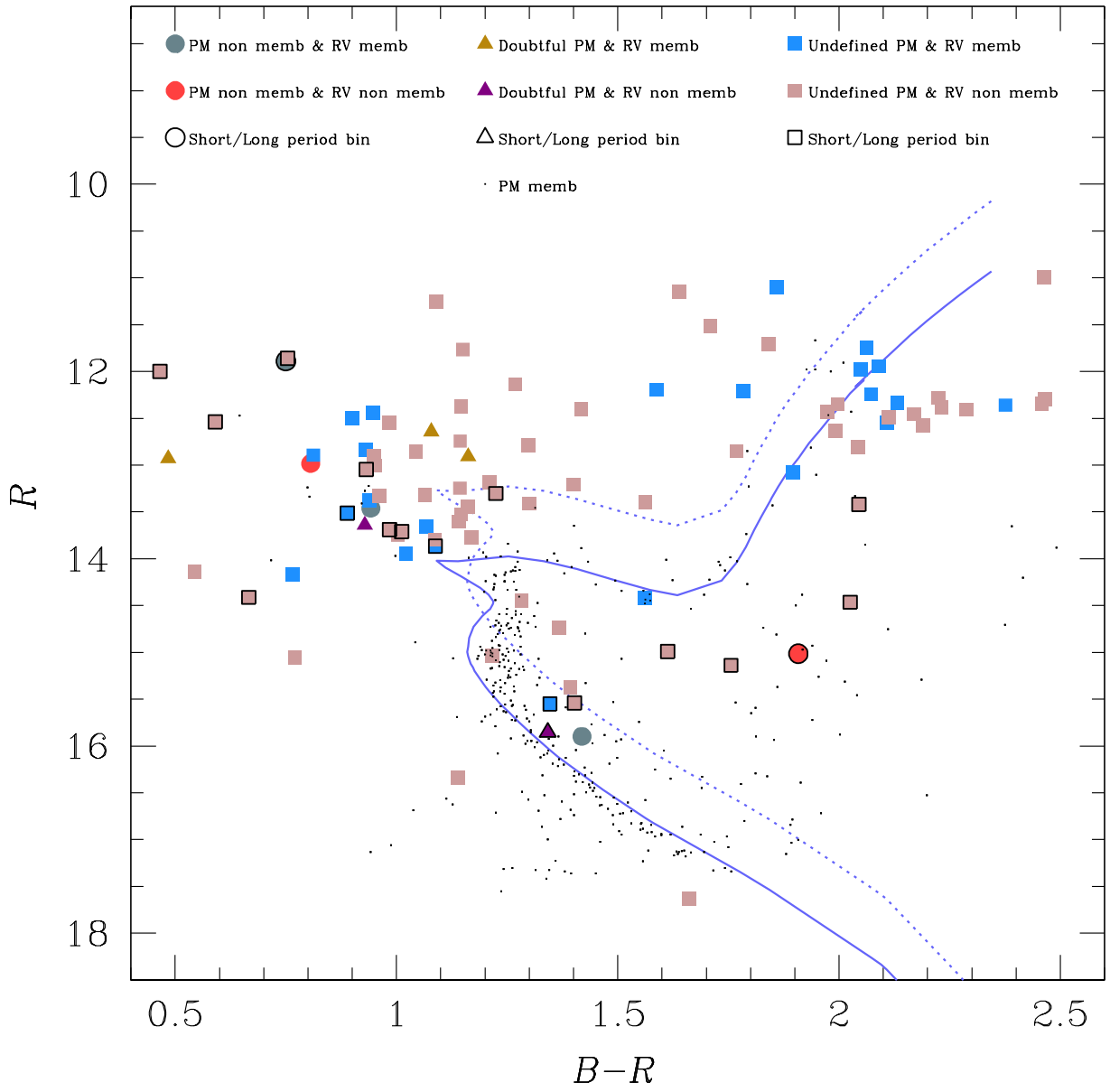

Fig. 5. Same as Fig. 4, but for proper motion non members or for stars which proper motion membership probabilities are either doubtful or absent, as explained in the legend.

4.6. Star 45474

Star 45474 is a proper motion and radial velocity cluster's member (MP=97%, $\overline{RV_{obs}}$-$\overline{RV_{cl}}$ =1.712σ_{cl} = 7.294 km/s) in the turn-off region, and a likely close binary system (σ_{obs} = 8.090 km/s, $\sigma_{obs}/\overline{\sigma_{obs}}$ = 28.360). This star was observed also by Sestito et al. (2007), that determined a radial velocity equal to (33.49 ± 2.87) km/s with a difference of 11.67 km/s with respect to our own mean radial velocity, confirming the binarity of the object.

4.7. Star 45413

Star 45413 at the red-clump, proper motion and radial velocity member (MP=91%, $\overline{RV_{obs}}$-$\overline{RV_{cl}}$ =0.884σ_{cl} = 3.767 km/s), does not present indication of binarity from our dataset (σ_{obs} =0.467 km/s, $\sigma_{obs}/\overline{\sigma_{obs}}$ =1.129), though a comparison with the measurement of Carretta et al. (2007) gives a difference of 12.207 km/s with respect to our mean radial velocity, suggesting that the star is a binary system.

4.8. Star 44682

Star 44682 at the turn-off, is a double-lined spectroscopic binary, probably with a period much longer than our observing window, since from our radial velocities this star is not variable (MP=95%; $\overline{RV_{obs}}$-$\overline{RV_{cl}}$ =2.774σ_{cl} = 11.819 km/s, σ_{obs} = 0.326 km/s, $\sigma_{obs}/\overline{\sigma_{obs}}$ = 1.079).

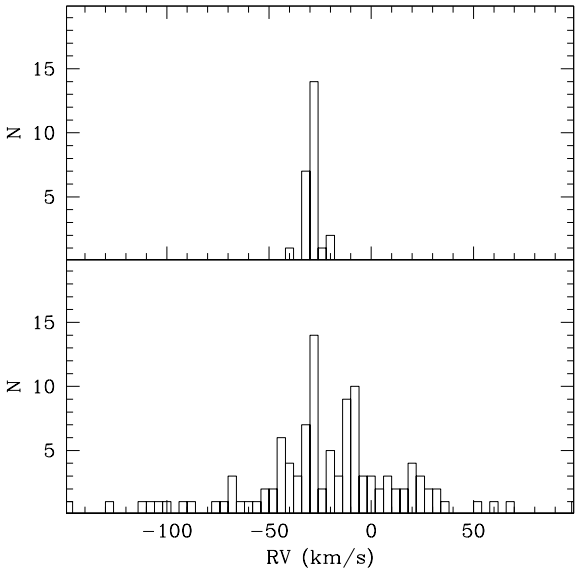

Fig. 3. Upper panel: radial velocity distribution of stars considered as cluster's members on the basis of proper motions and radial velocities; Bottom panel: radial velocity distribution of all the remaining stars in the sample (see text).

4.9. Star 45421

Star 45421 at the red-giant branch, was already classified as a potential binary star by Sestito et al. (2007). Our estimated mean radial velocity differs from their measurement by ∼ 2.7 km/s. It appears that this star is a likely cluster's close binary, though from our measurements it was not classified as a radial velocity variable star (MP=94%; $\overline{RV_{obs}}$-$\overline{RV_{cl}}$ =2.519σ_{cl} =10.730 km/s, σ_{obs} =0.339 km/s, $\sigma_{obs}/\overline{\sigma_{obs}}$ =1.389).

4.10. Stars 45404, 45412, 45414, 45410

These stars were observed also by Sestito et al. (2007, star 45404), and Carretta et al. (2009, stars 45412, 45414, 45410[4]). They are not RV variables, and our mean radial velocities agree with the measurements of those authors (within their uncertainties), and with our radial velocity cluster's membership criterium.

4.11. Proper motion members and radial velocity non members

Stars indicated by steel blue squares (Fig. 4) have mean radial velocities that do not satisfy our cluster's membership radial velocity criterium. They are in total six stars. Five of them are likely cluster's close binaries.

4.12. Star 44079

Star 44079, at the cluster's turn-off, (MP=90%; $\overline{RV_{obs}}$-$\overline{RV_{cl}}$ =5.392σ_{cl} = 22.968 km/s, σ_{obs} =35.258 km/s, $\sigma_{obs}/\overline{\sigma_{obs}}$ = 100.587) is a spectroscopic binary system. De Marchi et al. (2009) report that this star is a RS CVs star with period ∼2.18 days, and presents signs of activity and also a shallow eclipse (∼ 0.02 mag).

4.13. Star 45368

Star 45368, located at the sub-giant branch is an eclipsing binary double-lined system, as we determined by visual inspection of the light curve[5]. The binarity is also confirmed by our radial velocity measurements (MP=95%; $\overline{RV_{obs}}$-$\overline{RV_{cl}}$ =6.146σ_{cl} =26.183 km/s, σ_{obs} =109.131 km/s, $\sigma_{obs}/\overline{\sigma_{obs}}$ = 363.682). It will be discussed in more detail in Sect. 7.

4.14. Stars 45528

Star 45528 at the turn-off is a double-lined spectroscopic binary system (MP=97%; $\overline{RV_{obs}}$-$\overline{RV_{cl}}$ =14.690σ_{cl} =62.581 km/s, σ_{obs} =20.931 km/s, $\sigma_{obs}/\overline{\sigma_{obs}}$ = 70.842).

4.15. Stars 45403

Star 45403 at the turn-off is a double-lined spectroscopic binary system (MP=97%; $\overline{RV_{obs}}$-$\overline{RV_{cl}}$ =5.177σ_{cl} =22.054 km/s, σ_{obs} =39.078 km/s, $\sigma_{obs}/\overline{\sigma_{obs}}$ = 135.101).

4.16. Star 45300

Star 45300 is located close to the red-giant branch of the cluster. Its deviant radial velocity would suggest that this object could be a candidate cluster's close binary, although we have no possibility to check this hypothesis. From our radial velocities the object is not variable (MP=94%; $\overline{RV_{obs}}$-$\overline{RV_{cl}}$ =12.564σ_{cl} =53.524 km/s, σ_{obs} =0.256 km/s, $\sigma_{obs}/\overline{\sigma_{obs}}$ = 0.859).

4.17. Star 30341

Star 30341 is instead almost certainly a field contaminant with similar proper motion of cluster's stars, as indicated by its deviant radial velocity (MP=87%; $\overline{RV_{obs}}$-$\overline{RV_{cl}}$ =10.100σ_{cl} =43.025 km/s, σ_{obs} =1.277 km/s, $\sigma_{obs}/\overline{\sigma_{obs}}$ = 1.734), and position in the CMD. Note that its proper motion membership probability is the lowest among the sample of proper motion cluster's members listed in Table 3. De Marchi et al. (2009), classified this star as an eclipsing contact binary system (EW) with period 0.27 days, and semi-amplitude ∼ 0.02 mag. From our radial velocities, the object is not variable. Given the small dispersion of the radial velocity measurements, and the very small period determined photometrically, we argue that this object may be a rotational variable, rather than a contact binary. As stated in De Marchi et al. (2009), it is very difficult to distinguish between these two classes of variables from the photometry alone.

In summary, given the high proper motion membership probabilities of these stars, and their position in the CMD, it is likely to believe that their are all likely cluster's members (with the exception of star 30341). In particular, their deviant radial velocities could be explained by the large dispersions we observed for stars 44079, 45368, 45528, 45403, and by long periods and massive companions for stars 44682, 45421, and 45300,

[4] Star 45410 in common with Carretta et al. (2007), it is considered a proper motion cluster's member, although its position in the sky is slightly outside the region where we considered reliable our proper motions (Montalto et al. 2009).

[5] This object is not included in the list of variable stars of De Marchi et al. (2009)

4.18. Proper motion non members or stars with doubtful/undefined proper motions

In Fig. 5, we present the results for stars which are proper motion non members, or have doubtful/undefined proper motions, as indicated by the different symbols (see the legend). Different colors separate radial velocity members from non members. Framed symbols highlight close binaries among this sample. None of the few stars with proper motions met our selection criteria for cluster's membership, and most stars have undefined proper motions.

The median radial velocity of this sample of stars is RV_{field} = −8.98 km/s (excluding close binaries) and the root mean square of the residuals is σ_{field} = 48.40 km/s. Fitting a Gaussian function to this distribution we expect (9 ± 3) stars with radial velocity consistent with cluster's membership ($\overline{RV_{cl}}$ = −29.11± km/s, 12.78 km/s= $3\sigma_{cl}$). We count instead 14 potential radial velocity members. Looking at Table **??**, considering the radial distances of these objects from the cluster's center, and their positions in the color magnitude diagram, the most likely cluster's members are: the detached binary (EA) 31195, located in between the cluster's main sequence and the cluster's equal mass binary sequence (Fig. 5); the sub-giant branch star 25450_2; the blue straggler candidates 45392, 45396, 45409, 45427, and 45433. These candidate members must be considered with caution, since their proper motion membership probabilities are not very large (≤ 85%).

4.19. The frequency of binary systems

The frequency of binaries among cluster's and field stars can be investigated thanks to photometric (Montalto et al. 2009, De Marchi et al. 2009) and radial velocity results (Sestito et al. 2007, Carretta et al. 2007 and this work). We consider a star as a likely binary system if either the photometry[6] or the spectroscopy allowed us to classify the star as a binary.

Among our sample of 35 likely cluster's members, we found that 12 objects are likely cluster's binary systems giving a binary frequency of f_{bin} =(34±10)%, where the error accounts for Poisson statistic[7]. The frequency remains essentially inaltered including also the sample of 7 stars indicated in the previous paragraph as likely members (among which two are variables), f_{bin} =(33±9)%. This result is in good agreement with previous estimates (e. g. Bragaglia et al., 1997; Montalto et al., 2009), though it is certainly underestimating the real value, since in general we are not complete for long period binary systems and very small mass companions.

However, an homogeneous comparison with the field's binary frequency can be done only for binaries detected from our own surveys (both photometric and spectroscopic), since no field objects were spectroscopically observed by other authors in the past years. Just to distinguish the frequency of these binaries from the previous estimate, we use here the term *frequency of close binaries* (f_{cl}), because both our photometric and spectroscopic surveys covered a few nights of observations.

Then 10 stars out of 35 are likely cluster's close binary systems of NGC 6253, which gives: f_{cl} =(29±9)% (or 29%±8% considering the seven stars in the previous paragraph) for the cluster, and equal to $f_{cl,field}$ =(22±5)% (excluding the seven stars of the previous paragraph) for the field. Our estimated cluster's binary frequency appears then higher than the field binary frequency, although they are consistent within the uncertainties. We note also that the sample of cluster's stars analyzed is still small, and there may be some selection effects. De Marchi et al. (2009) observed that the class of main-sequence rotational variables is the most numerous, as observed in the surrounding field of NGC 6253. In our sample, there are in fact only two rotational variables. More in general, in this work we focused on the binarity of turn-off stars, and evolved stars, whereas the study of De Marchi et al. (2009) analyzed the variability of fainter objects.

Mermilliod et al. (2009) obtained an overall binary frequency equal to 30% from the analysis of 13 nearby open clusters, considering their 19-years CORAVEL survey, which would be consistent with our estimates.

Mathiew R. D. et al. (1990) derived a frequency of binaries with periods less than 1000 days comprised between 9% and 15% among the solar mass M67 members. Latham et al. (2002) obtained a frequency equal to (15.8 ± 1.5) % for the halo population finding no obvious difference with the disk populations. An accurate comparison of our results with previous literature findings is beyond the purpose of this work, however we note that our estimated frequency of close binary systems (f_{cl}) appears somehow higher than what derived by these authors in other environments, even if the difference is only significant at ∼1.6-σ, considering our errors.

5. Transiting planetary candidates

In this Section, we present a preliminar analysis of the three planetary transiting candidates we found in the field of NGC 6253, based on the photometry data acquired at the La Silla 2.2m Telescope, and on the UVES spectroscopy. In Fig. 6, we present the color magnitude diagram of proper motion cluster's members together with the colors and magnitudes of the transiting candidates. None of these candidates is located in the region were our proper motions are reliable. Moreover, from Fig. 6, it appears that only star 171895 may be compatible with cluster's membership, since it is located in the turn-off region. The other objects are likely field stars.

5.1. Star 171895

The magnitude of the target star is V = 15.260 ± 0.002. From the analysis of the UVES spectra, we obtained the following parameters: T_{eff} = 5720 ± 50K, log(g) = 4.50 ± 0.20, [Fe/H] = +0.36 ± 0.02. Using these parameters and uncertainties and the isochrones with metallicity Z = 0.03 with ages comprised between log(age[Gy]) = 7.8 and log(age[Gy]) = 10.25 taken from the Padova database we constrained the mass, radius and age of the star obtaining: M = (1.07 ± 0.04)$M_\odot$, R = (1.04 ± 0.07)$R_\odot$ and age = (8.9 ± 0.7) Gyr.

In Fig. 7 (upper panels) we present the entire lightcurve of the object obtained using the WFI data. The photometry of the 2009 observing season was more noisy than the photometry of 2004, since we observed in April (at tipically higher airmasses than in June 2004), and during bright time (dark time in 2004). However, we detected three evident transit events (denoted by the roman numbers I, III, and IV in Fig. 7) of around 0.024 mag depth. The first (full) transit was detected in 2004, the other two (a partial transit during the flat bottom region and a full transit)

[6] We did not considered in the binary list pulsational variables like RR Lyrae, and δ Scuti stars.

[7] Star 30341 is considered a field star, and star 45300 is considered a long period cluster's binary.

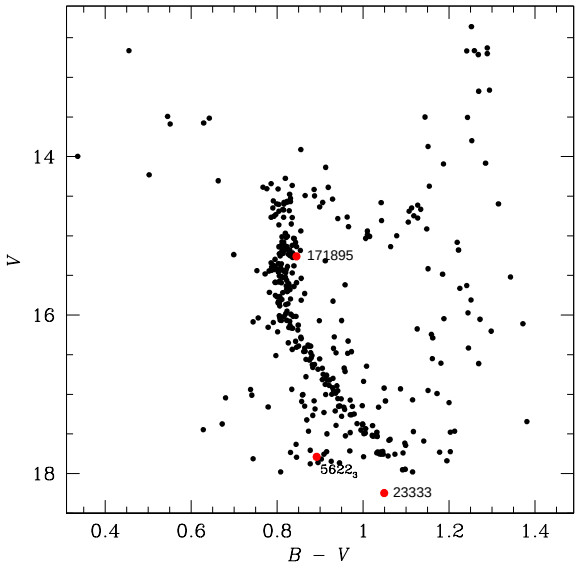

Fig. 6. V, $B-V$ color magnitude diagram of proper motion cluster's members of NGC 6253, with highlighted the positions of the three planetary transiting candidates discussed in the text.

in 2009 [8]. The period of the transiting object was deduced using at first the two transits of 2009, which allowed us to guess the closest integer period to the real period (that is four days), and then folding the lightcurve finding the best solution consistent with all our photometric measurements and able to overlap the two full transits. We assumed a *constant* period. The result is P = 4.16164 days. Submultiples of this period are then excluded by our photometry. On the basis of this procedure we also deduced that a few photometric measurements acquired just at the end of the nineth night in 2004 should have been located just at the ingress of the transit (see the epoch denoted by the roman number II). In the folded lightcurve presented in Fig. 7 (bottom left panel) we note that the points acquired during that night (open circles) present a slight photometric offset with respect to the other measurements ($\sim$ 0.002 mag), and that the two points just inside the transit present relatively large residuals with respect to the best transit model matching the observations denoted by the red, even accounting for the photometric offset. Wether this is an indication that assuming a *constant* period is not correct it is not clear from these observations. A few other measurements acquired during epoch IV (open boxes) and with similar phases ~ -0.05 days in the same Figure, appear to have large residuals as well, however this is more likely due to the lower photometric quality of the 2009 observing season. Other photometric measurements are cleary necessary to clearly understand this system.

The best-fit model was obtained using the Mandel & Agol (2002) algorithm, and a quadratic limb darkening law, where the limb darkening coefficients were selected from the table of Claret (2000) accordingly to the spectral type of the host star. The stellar parameters (mass and radius) were also fixed to the mean values we obtained from spectroscopy. The model well reproduces the shape of the observed transits. The RMS of the fit is 0.002 mag, the radius of the transiting object we obtained is $R_{pl} = 1.49\,R_{jup}$, and the inclination 87°.

The UVES radial velocity measurements are shown in Fig. 7 (lower right panel), and presented in Table 2. Since we did not know the orbital period at the time of the UVES observations (only one transit was detected in 2004, see above), it was not possible to accurately plan the spectroscopic follow-up of this object. The UVES measurements were unfortunately acquired at very similar orbital phases, as shown in Fig. 7 (lower right panel). As a consequence it is not possible to derive an orbital solution. The measurements are compatible within their errors, which is 200 m/s. Observations at other orbital phases and of higher precision are necessary to accurately constrain the mass of the transiting object. The epoch (E) of the eclipses is given by:

$$(HJD - 450000.) = 3162.15268 + 4.16164 \times E.$$

Table 2. Journal of UVES data for star 171895.

Epoch	HRV(km/sec)	err_{HRV}(km/sec)
2454695.53216	-51.00	0.2
2454699.53815	-50.55	0.2
2454703.54365	-50.88	0.2

5.1.1. Cluster's membership

As demonstrated above, star 171895 is a very metal rich star, and it appears located in the cluster's turn-off region. Since the target star has no proper motion in our own catalog (see above), we retrieved proper motions from the UCAC2 catalog. In particular we cross-matched our catalog with UCAC2, isolating likely cluster's members on the basis of our proper motions. In Fig. 8, we show the proper motion of the target star (red point), together with the (UCAC2) proper motion of likely cluster's members (big black dots), and with those of likely field stars with radial distance from the cluster's center comprised between $10'$ and $40'$. The median values and the standard deviations of the right ascension and declination proper motion distributions are $\overline{\mu_\alpha} = -78$ mas/yr, $\overline{\mu_{\delta\,cos(\delta)}} = -77$ mas/yr, $\sigma_{\mu_\alpha} = 153$ mas/yr, $\sigma_{\mu_{\delta\,cos(\delta)}} = 141$ mas/yr, for likely cluster's members, and $\overline{\mu_\alpha} = -30$ mas/yr, $\overline{\mu_{\delta\,cos(\delta)}} = -67$ mas/yr, $\sigma_{\mu_\alpha} = 179$ mas/yr, $\sigma_{PM_{\delta\,cos(\delta)}} = 116$ mas/yr for likely field stars. The proper motion of the target star is $\mu_\alpha = 30$ mas/yr, $\mu_{\delta\,cos(\delta)} = -197$ mas/yr. From these numbers it appears that UCAC2 proper motions are not very effective in distinguishing among field and cluster's stars given the large errors. The proper motion of the target star is consistent within $0.7\sigma_{\mu_\alpha}$, and $0.85\sigma_{\mu_{\delta\,cos(\delta)}}$ with the likely cluster's members distribution and within $0.3\sigma_{\mu_\alpha}$, and $1.12\sigma_{\mu_{\delta\,cos(\delta)}}$ with the likely field stars distribution. However, the mean radial velocity of the system is equal to -51.81 km/s, which is *not* consistent with the recession velocity of the cluster ($\overline{RV_{cl}} \pm \overline{\sigma_{cl}} = -29.11 \pm 0.85$ km/s), and its location in the sky is rather distant from the cluster's center (16.2 arcmin).

Given the present observations the most likely interpretation is that star 171895 is a very metal-rich field star falling by coincidence just at the cluster's turn-off. The presence of an additional close stellar companion in the system (e.g. a 0.8 $M_\odot$ star on a $\sim$ 100 days orbit, and presumably a white dwarf since we did not detect double peaks in the cross-correlation function) would be required to reconcile the disagreement between the mean radial velocity of this star and the recession velocity of the cluster.

[8] The 2009 photometric observations will be accurately described in a forthcoming paper, they have been obtained thanks to Max Planck Institute for Extraterrestrial Physics reserved time.

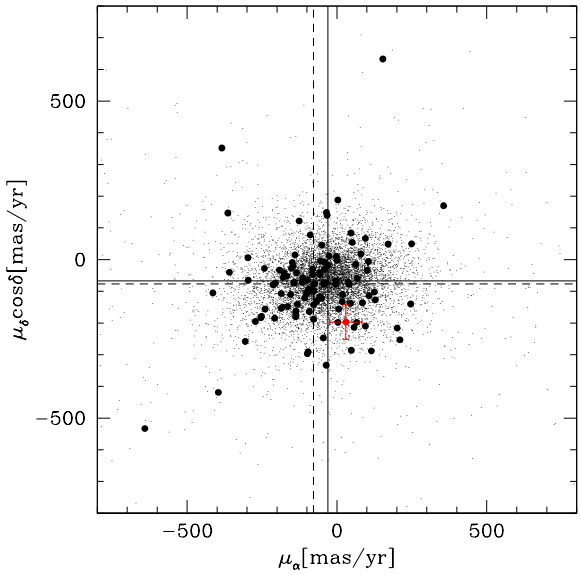

Fig. 8. UCAC2 proper motion diagram. Big black points denote likely cluster's members (see text). Small black dots stars with radial distance from the cluster's center comprised between $10'$ and $40'$, and the red dot the proper motion of star 171895. The dashed lines indicate the median proper motion of cluster's stars, and the continuous lines the median proper motion of field stars.

Such scenario appears quite unlikely, otherwise since additional radial velocity measurements are necessary to constrain the mass of the transiting objects, this further hypothesis can be automatically checked. The HARPS instrument will perfectly accomplish these tasks, since we expect a precision of 10 m/s with 1 h of integration time for this star.

5.2. Star 5622_3

The magnitude of the host star is $V = 17.789$. Its radial distance from the cluster's center is 18.5 arcmin. In our photometry we detected 8 transit events with a periodicity of 0.8494083 days, (Fig. 9, upper panels). No UVES measurements were acquired for this system. This was probably due to a bad positioning of the fiber, considering also the faintness of the object. The transits depth is ∼ 0.008 mag. Assuming that the host is a solar-type star we obtained the best-fit shown by the red line in Fig. 9 (bottom panel). The RMS of the fit is 0.003 mag, the radius of the transiting object is R =0.82 R_{jup}, and the inclination is 85°. We observe that the ingress and egress phases do not appear to closely follow the model, although the large scatter does not allow to draw a definitive conclusion. The epoch (E) of the eclipses is given by:

$$(HJD - 450000.) = 3168.99730 + 0.8494083 \times E.$$

Since we are not able to characterize spectroscopically the host star, no additional informations on this system are provided here.

5.3. Star 23333

The magnitude of the host star is $V = 18.247$. This object is the closest to the cluster's center, with a radial distance of 6.4 arcmin. From our photometry we detected 4 transits events, 2 full transits in 2004 and 2 partial transits in 2009 (Fig. 10 upper and lower left panels). Given the faintness of the object the lightcurve is very noisy. The transits are rather deep, being around 0.03 mag, and the duration is ∼ 1.92 hours. The folded radial velocity measurements are shown in the bottom right panel of Fig. 10. In this case radial velocity measurements would be sufficiently well separated in phase space to derive some orbital constraints. However, the error of each measurement is large (∼ 3.6 km/s). Even when binning the couple of datapoints we acquired at the same orbital phase, the error is reduced by a $\sqrt{2}$ (2.5 km/s). More importantly, from the UVES spectroscopy we were able to derive an approximate value of the effective temperature of the host star, which is T_{eff} = (5700 ± 200) K. We were not able to derive the gravity since the low S/N of the spectra. However, given that effective temperature, and assuming that the host is a dwarf star, we obtained that the transits are too deep to be determined by a planetary body. The best fit obtained with the Mandel & Algol (2002) algorithm, considering a solar type host star, would give a radius for the secondary equal to 2.25 R_{jup} and an inclination of 84°. This is sufficient to exclude this object from the list of planetary transiting candidates.

Among the three planetary transiting candidates presented, star 171895 is the most interesting object, both for its brightness and for its characteristics. Follow-up observations of this system (both photometric and spectroscopic in particular with the HARPS instrument) are clearly warranted to accurately determine its properties.

Table 3. Journal of UVES data for star 23333.

Epoch	HRV(km/sec)	err_{HRV}(km/sec)
2454695.56104	-16.254	3.627
2454695.53224	-14.608	3.710
2454699.50991	-12.687	3.627
2454699.53824	-12.442	3.710
2454703.54373	-12.193	3.710
2454703.51466	-13.425	3.627

6. Detached eclipsing binary systems

Among the objects in our target list there are four known detached eclipsing binary systems (see Sect. 1). These objects were selected from the list compiled by De Marchi et al. (2010). As it appears evident from their Table A.3 several of these detached systems present very shallow eclipses. In particular, six objects in their list have eclipses with aplitudes ≤ 0.03 mag. We decided to target with the GIRAFFE spectrograph star 31195, 126376, 38138, and 24487, which have eclipses of amplitudes 0.02 mag, 0.02 mag, 0.01 mag, and 0.53 mag, and periods equal to 1.8156 days, 1.5896 days, 0.66606 days, and 0.85120 days respectively. The lightcurves of these objects were already presented in De Marchi et al. (2010). They tipically show out of eclipse modulations, with the presence of primary and secondary eclipses. The eclipses are also markedly V-shaped. The only exception may be star 38138, where the eclipses are shallow and noisy and not easily distingishable from each others. Assuming that the obseved transits are grazing eclipses caused by very close stellar companions (given the short periods), we should expect to observe large radial velocity variations. For example, a stellar companion just at the limit between the brown dwarf and the stellar regime (M=0.08 $M_\odot$) in a circular orbit with period equal to P = 1.8156 days would produce a radial velocity semi-amplitude equal to K = 12.5 km/s (assuming the primary star is

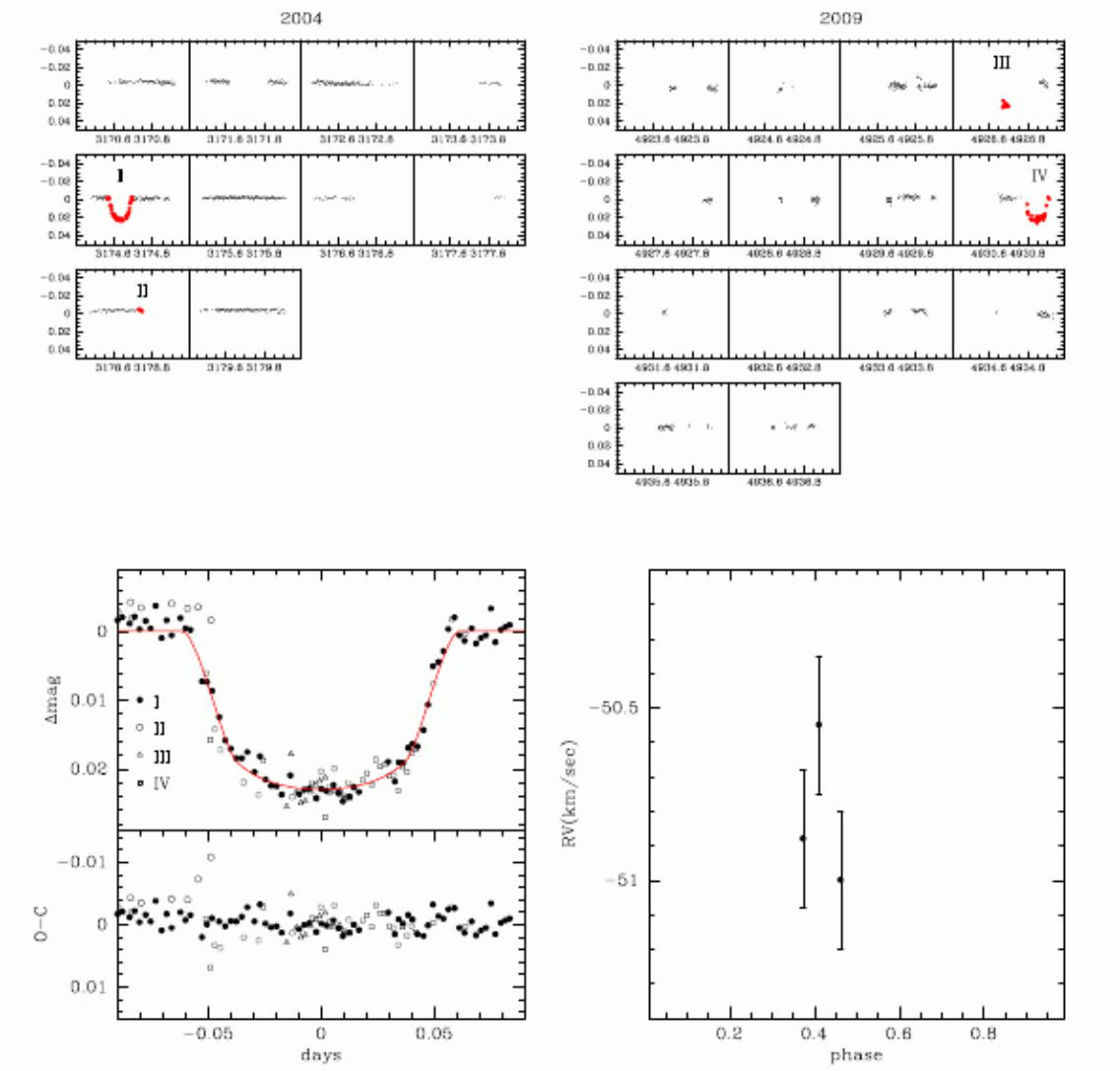

Fig. 7. *Upper left:* lightcurve of star 171895 relative to the 2004 observing season. Red points highlight transit epochs, also indicated by the roman numeration. *Upper right:* lightcurve of star 171895 relative to the 2009 observing season. *Lower left, top panel:* folded lightcurve. The continuous line indicates the best-fit model obtained using the Mandel & Algol (2002) algorithm, considering as properties of the host star those derived from the UVES spectroscopy. The roman numeration and the associated symbols are relative to the transit epochs shown in the upper panels. *Lower left, bottom panel:* observed minus model residuals. *Lower right:* UVES spectroscopic measurements.

a solar type star). From Table **??** we see instead that only star 24487 has been detected as a binary in our spectroscopic survey. In other words all the three objects presenting shallow eclipses did not appear radial velocity variables. For star 38138 the observations have been acquired almost at the same phase (0.16, 0.17, 0.19 in chronological order and assuming the time of minimum and the period reported in Table A.3 of De Marchi et al. 2010). For star 127376 the phase is also close to 0 or 0.5 (0.06, 0.58, 0.1). However, it appears that for star 31195 we should have reasonably expected to detect a large radial velocity variations since the observations were acquired at orbital phases equal to 0.11, 0.31, and 0.52. One possible explanation is that star 31195 is in fact a hierarchical triple system, or a blend, where a third unresolved companion determined shallower eclipses, and fictitiously small radial velocity variations. Since, as we discussed in Sect. 4 and also pointed out by De Marchi et al. (2010), this object might be considered a likely cluster's member despite its proper motion membership probability is not very high, it would be very important to acquire other observations to better clarify its nature.

7. The eclipsing binary system 45368

Star 45368 is a double-lined eclipsing binary system located at the sub-giant branch of NGC 6253, and it is a very likely cluster's member as indicated by its proper motion and position in the CMD (see Sect. 4). In Fig. 11, we present the photometric observations acquired for this object, distinguishing between 2004 (black points) and 2009 (open red circles) observations. We detected in total four eclipses, all of them partial during the ingress of the transits. Moreover, as seen in Fig. 11, the lightcurve is not constant out of the eclipses, since there are some clear light modulations. The 2009 observations appear also in this case of lower quality with respect to the observations acquired in 2004.

The UVES measurements presented in Fig. 12 indicate a very large radial velocity variation ($\sigma_{obs}/\overline{\sigma_{obs}}$ = 363) consistent

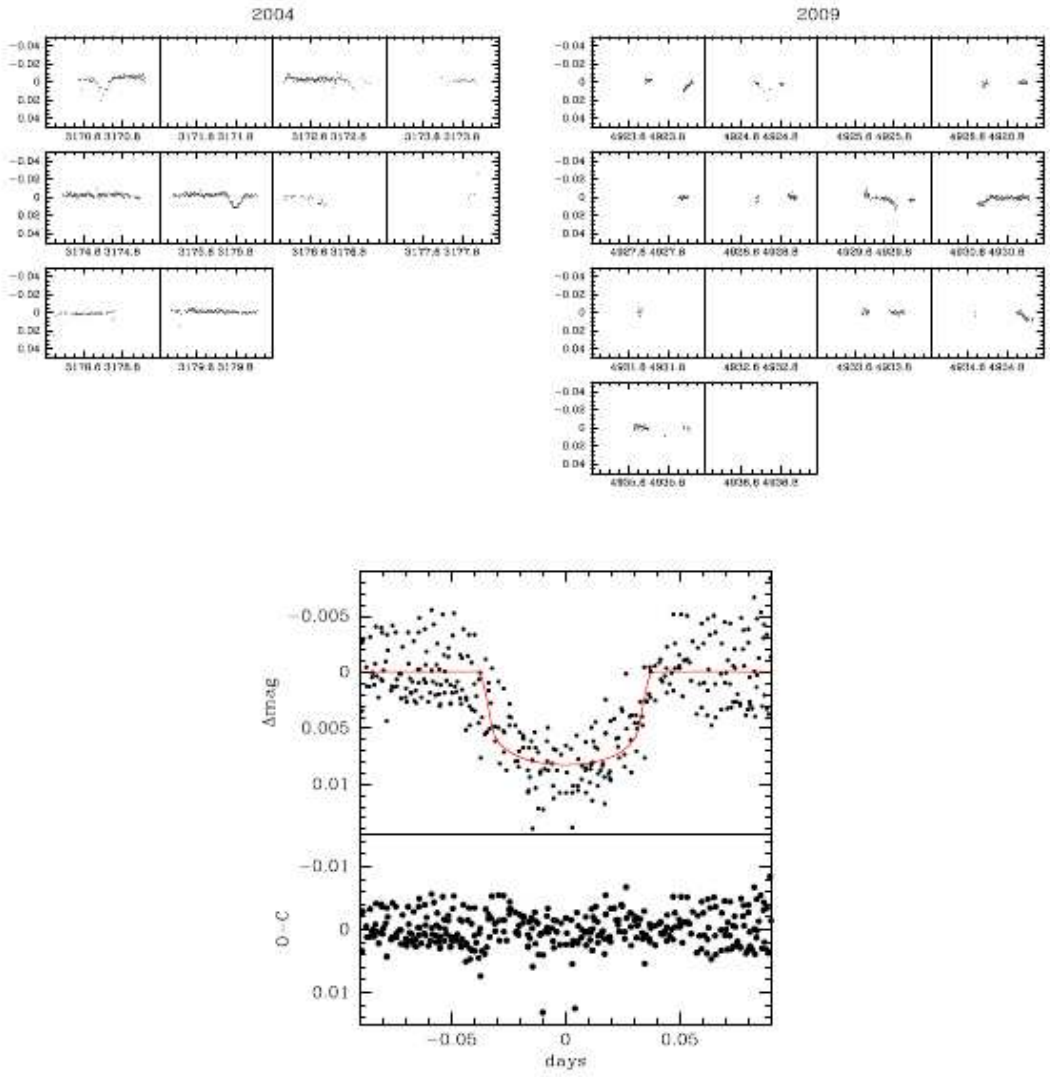

Fig. 9. *Upper left:* lightcurve of star 5622_3 relative to the 2004 observing season. *Upper right:* lightcurve of star 5622_3 relative to the 2009 observing season. *Lower panel, upper figure:* folded lightcurve. The continuous line indicates the best-fit model obtained using the Mandel & Algol (2002) algorithm, assuming that the host star is a solar type star. *Lower panel, bottom figure:* observed minus model residuals.

with the idea of a stellar binary system and a short orbital period. Filled circles represent the heliocentric radial velocities of the primary star, and open circles of the secondary. The data are presented in Table 4. Our result for the epoch (E) of the primary eclipse is:

$$(HJD - 450000.) = 3178.2903(1) + 2.57317(1) \times E$$

In Fig. 12, we fit the radial velocity measurements with the following models:

$$RV1_{sim}(km/s) = 0.2\ \ m2\ sin(i)\ P^{-1/3}(m1+m2)^{-2/3} \times \\ \times\ cos\Big(\frac{2\pi}{P}\,(t - 3178.2903470538) + \frac{\pi}{2}\Big) + \gamma \qquad (6)$$

$$RV2_{sim}(km/s) = 0.2\ \ m1\ sin(i)\ P^{-1/3}(m1+m2)^{-2/3} \times \\ \times\ cos\Big(\frac{2\pi}{P}\,(t - 3178.2903470538) + \frac{3}{2}\pi\Big) + \gamma \qquad (7)$$

where $m1$ and $m2$ are the masses of the primary and the secondary stars both in solar masses, P is the period in days, t is the epoch of the UVES observations in days, γ is the barycentric velocity of the system, i the inclination of the system (assumed equal to 90°), and the result is given in km/s. We assumed a circular orbit since the short orbital period should imply tidal circularization. The two radial velocity curves represented by Eq. 6 and Eq. 7 are in phase with the observed times of the primary and secondary eclipses respectively. We varied the two masses between 0.6 $M_\odot$ and 10.5 $M_\odot$ in steps of 0.1 $M_\odot$, and γ between ± 4 km/s from the recession velocity of the cluster (−29.11 km/s) in steps of 40 m/s. The best solution was found minimizing the quantity:

$$\chi^2 = \frac{\sum_{i=1}^{i=3}(RV1_i - RV1_{sim,i})^2/\sigma^2_{RV_i}}{N-3} + \\ + \frac{\sum_{i=1}^{i=3}(RV2_i - RV2_{sim,i})^2/\sigma^2_{RV_i}}{N-3} \qquad (8)$$

where $RV1_i$, $RV2_i$, are the observed radial velocities of the primary and of the secondary respectively, σ_{RV_i} are the uncertainties of the radial velocity measurements as reported in Table 4

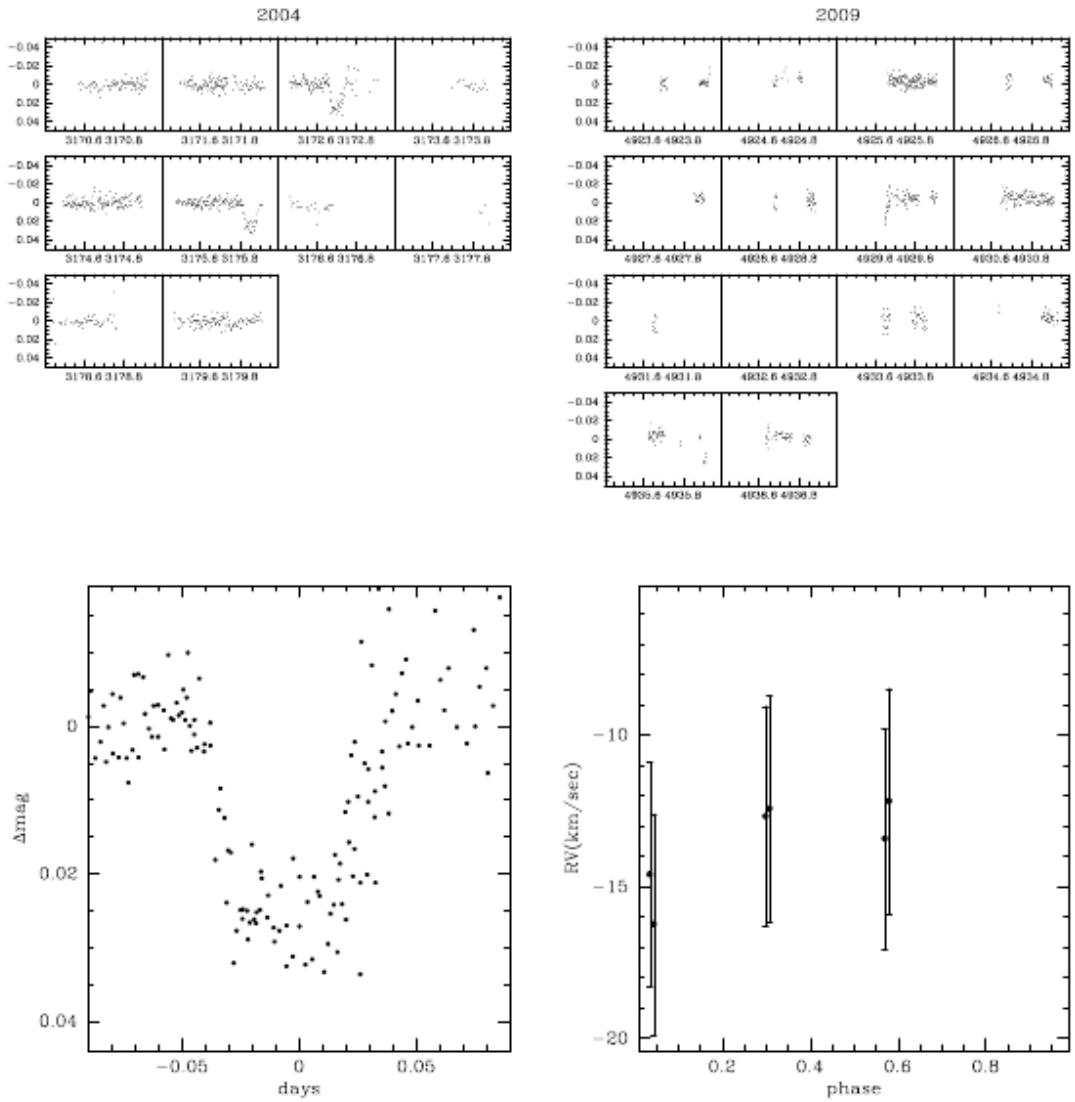

Fig. 10. *Upper left:* lightcurve of star 23333 relative to the 2004 observing season. *Upper right:* lightcurve of star 23333 relative to the 2009 observing season. *Lower left:* folded lightcurve. *Lower right:* UVES spectroscopic measurements.

Table 4. Journal of UVES data for the 45368 eclipsing binary system.

Epoch	HRV1(km/s)	HRV2(km/s)	σ_{HRV}(km/s)
2454695.53216	45.43	-109.96	2.809
2454699.53815	-128.21	74.08	2.417
2454703.54365	73.40	-141.71	3.464

and $N-3=3$ since we have six independent measurements, and three degrees of freedom ($m1$, $m2$, and γ). The result of the fit is represented by the solid and the dotted curves in Fig. 12 relative to the primary and secondary star respectively, and implies $m1 \sim 1.6\,M_{\odot}$, $m2 \sim 1.5\,M_{\odot}$, $\gamma = -30.2$ km/s, and $\chi = 1.23$. The value of the barycentric velocity of the system is then fully consistend with cluster's membership, leaving little doubt that the system belongs to the cluster. The masses we derived confirm also the idea that these stars are cluster's evolved objects as suggested by the position along the sub-giant branch of the cluster, and by the fact that turn-off stars have masses around $\sim 1.3\,M_{\odot}$, as derived by isochrone fitting.

In Table 5, we summarize the results obtained from our analysis. Since in our photometry the two eclipses are only partial, we did not try to fit the lightcurve of this system and constrain the radii of the stars. We note that between the 2004 and 2009 measurements there could be a photometric offset. However, a complete and detailed analysis of this system will be presented once more data will be available. The possibility to derive accurate masses and radii for these evolved stars will offer an excellent oppotunity to test stellar evolution models predictions at the extreme metallicity of NGC 6253.

Table 5. Summary of the parameters derived for the 45368 eclipsing binary system, assuming $i = 90°$ and $e = 0$.

Period(days)	2.57317(1)
HJD of primary eclipse	2453178.2903(1)
γ(km/s)	-30.19
$m2/m1$	0.94
$m1(M_\odot)$	~1.6
$m2(M_\odot)$	~1.5

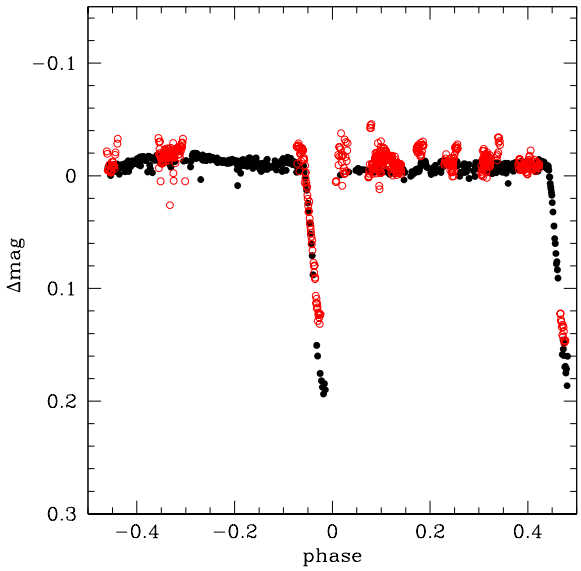

Fig. 11. Folded light curve of the eclipsing binary system 45368. Black filled points are relative to the 2004 observing season, and red open circles to the 2009 observing season.

8. Radial velocity searches for sub-stellar companions around old open clusters turn-off stars

In this Section, we estimated the number of planets we can expect to detect during a radial velocity survey toward NGC 6253, considering different observing strategies. We focused our attention on cluster's turn-off stars ($V = 15$), and assumed to use the HARPS spectrograph. At the magnitude of our target stars, considering 1 h of integration time for each star, we expect a radial velocity precision of 10 m/s per measurements. A 3-σ detection threshold implies that only substellar companions inducing radial velocity semi-amplitudes variations $K > 30$ m/s could be detected. From the Fischer & Valenti (2005) law we expect ~ 18% FGK dwarf stars having planets producing radial velocity semi-amplitudes $K > 30$ m/s, and with orbital periods up to 4 years, at the metallicity of NGC 6253 ([Fe/H=+0.39). We used the following Equation to simulate the observations of a planet-host star at some fixed epochs:

$$RV_{sim}(m/s) = 200 \;\; m \;\; sin(i) P^{-1/3} M^{-2/3} cos(n\tau + \phi) \qquad (9)$$

where n is the mean orbital motion ($= 2\pi/P$), and τ corresponds to the 3 epochs of our observations. In the above Equation, the period is expressed in days, the mass of the companion (m) in Jupiter masses, the mass of the primary (M) in solar masses, and the resulting radial velocities are in meters per second. Cluster's stars with the same magnitude of our targets have masses of

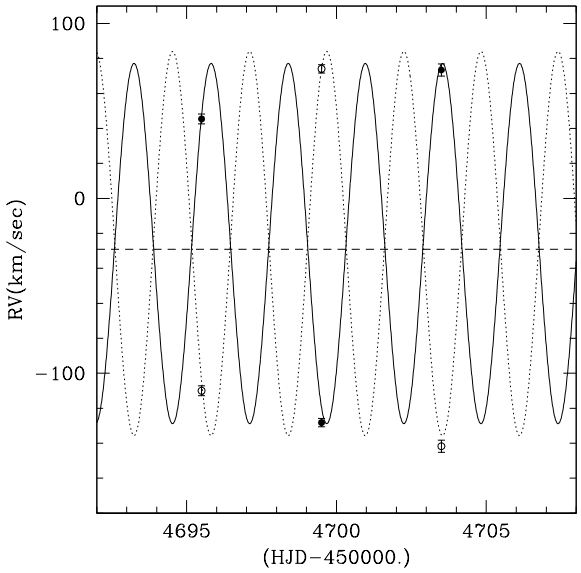

Fig. 12. Fill black circles and open circles are UVES radial velocity measurements of the primary and secondary components of the 45368 binary system. The solid curve is the best fitting model in phase with the primary eclipses. The dotted line is the best fitting model in phase with the secondary eclipse. The dashed horizontal line indicates the baricentric velocity of the system ($\gamma = -30.19$ km/s).

$\sim 1.3 M_\odot$ (derived from isochrone fitting), and we adopted this value for the primary's mass. Random gaussian scatter was also added to the measurements to account for observational errors (the dispersion was fixed to 10 m/s). The orbital period of the planet was varied between 1 day and 1460 days (= 4yr) in steps of 0.5 days, and the mass of the secondary between 0.5 M_{jup} and 13 M_{jup}, in steps of 0.1 M_{jup}. These limits are consistent with the validity domain of the Fischer & Valenti (2005) law. For each couple of period and mass we performed 1000 simulations randomly varing the orbital phase of the planet, and defined the detection efficiency (eff) as the ratio between the number of simulations for which the standard deviation of the simulated measurements around their mean value exceeded $3 \times \sigma = 30$m/s, with respect to the total number of simulations.

In order to calculate the expected number of planets, we convolved the detection efficiency with the mass-period functions of extrasolar planets as derived by Jiang, I.-G. et al. (2010). We considered the results obtained by those authors for independent mass functions, and in particular for the case of the single imaginary survey. Assuming coupled mass-period functions gives similar results, at least for the case of the single imaginary survey, as can be deduced from their Table 5. In such a way the probability (dP) that a single star of metallicity [Fe/H] has a planet with orbital period comprised between P and $P + dP$, and mass comprised between M and $M + dM$ is given by:

$$dP = c \left(\frac{M}{M0}\right)^{-\alpha} \left(\frac{P}{P0}\right)^{-\beta} \frac{dM}{M} \frac{dP}{P} \times 10^{2[Fe/H]} \times eff(M,P) \qquad (10)$$

where $\alpha = -0.143$, $\beta = -0.124$, $c = 0.001316$, $M0 = 1.5\, M_{jup}$, and $P0 = 90$ days. The efficiency function ($eff[M,P]$) depends not only on the mass and period of the orbiting planet, but also on the observing strategy. In the above Equation we have assumed that the mass-period functions are independent

Table 6. Number of detectable planets from different HARPS simulated observing runs. The results below are given assuming a total number of surveyed turn-off stars of NGC 6253 equal to 26.

N.sim	Epochs (days)	N.Planets
1	t1=1;t2=2;t3=3	1.42
2	t1=486;t2=972;t3=1458	3.23
3	t1=1;t2=2;t3=730	3.06
4	t1=1;t2=2;t3=3;t4=4;t5=5;t6=6	1.73
5	t1=1;t2=2;t3=729;t4=730;t5=1459;t6=1460	3.58
6	t1=1;t2=243;t3=486;t4=729;t5=972;t6=1215	3.87

from the host-star's metallicity, and from the host-star's mass. Ribas & Miralda-Escudé (2007) derived that the host star metallicities decrease with planet mass, however the significance of this result is only marginal considering the present sample of exoplanets. A dependence of planet's mass and orbital period on the planet's host mass has been also demontrated. In particular around M-dwarf stars hot-jupiter planets appear relatively rare (e.g. Endl et al. 2006), whereas they seem more frequent around giant stars with respect to dwarf stars, having long orbital periods, and rather large minimum masses (e.g. Sato, B. et al. 2007). Our considerations are however limited to neptune-jupiter planets around dwarf stars at the cluster's turn-off, then are not affected by this problem. Once applied to the period-mass domain of our simulations (see above), assuming solar metallicity and perfect efficiency ($eff = 1$), Equation 8 gives a detection probability of 3.1%, in good agreement with the normalization factor of the Fischer & Valenti (2005) law (3%). Once particularized to our case, assuming the metallicity of NGC 6253, the above Equation allows to calculate the total number of detectable planets and their distribution in period and mass, as reported in Table 6 and shown in Fig. 13 and Fig. 14. The main result is that the observing strategy has a large impact on the expected number of planets. With 3 epochs equally distributed over 4 years, and assuming an initial sample of 26 stars (which means a total of 78 HARPS hours) we can expect to detect 3.23 planets. If taken consecutively, we could expect to detect only 1.42 planets. In general, strategies that involve non consecutive observations are the most effective since they allow higher sensitivity to longer period planets.

9. Minimum mass and period of companion objects of cluster's members close binary systems

In this Section we studied the opposite problem of Section 8: assuming to find a radial velocity variable star during an *RV* survey and assuming that this variation is determined by the presence of a companion object, which are the most likely minimum mass ($m\,sin[i]$) and period (P) of this object? The effectiveness of an observing strategy should be evaluated not only considering if it is able to maximize the number of detectable planets, but also considering if it is able to minimize the number of spurious objects that may produce the same signal of the planets.

As an illustrative example, we considered at first the case of the *UVES* observations, and in particular of star 39810, which has the smallest dispersion among our sample of cluster's candidate close binary systems, as shown in Sect. 4. In Fig. 15, we present a comparison between the radial velocity measurements of star 39810 and of star 40519, which is also a turn-off cluster's member and not a radial velocity variable star. In this Figure, dotted lines indicate the stars' mean radial velocities ($\overline{RV_{obs}}$), solid lines represent the mean radial velocity of the cluster ($\overline{RV_{cl}}$), and dashed lines represent the 1 $\overline{\sigma_{cl}}$ uncertainty range of the cluster's mean radial velocity ($\overline{\sigma_{cl}}$ = 0.85 km/s, Sect. 4). While star 40519 radial velocities are all consistent with the cluster's recession velocity, measurements for star 39810 clearly depart from it. We assume in the following that the observed radial velocity variation for star 39810 is determined by the presence of a companion object. On the basis of this hypothesis, we constrain the expected minimum mass and period of this object by means of Monte Carlo simulations. The basic condition that we imposed is that the barycentric radial velocity of the binary system is coincident with the recession velocity of the cluster. This is possible thanks to the fact that this star is a very likely cluster's member, as demonstrated in Section 4. Was this object a common field star, we wouldn't have had any a priori knowledge on its barycentric radial velocity.

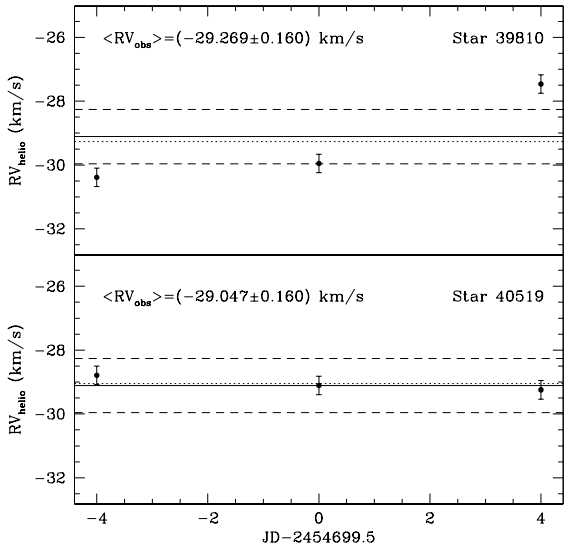

Fig. 15. Radial velocities obtained for stars 39810 and 40519 located in the turn-off region. Dotted lines indicate the stars' mean radial velocities ($\overline{RV_{obs}}$), solid lines represent the mean radial velocity of the cluster ($\overline{RV_{cl}}$), and the dashed lines represent the 1 $\overline{\sigma_{cl}}$ uncertainty range of the cluster's mean radial velocity ($\overline{\sigma_{cl}}$ = 0.85 km/s, Sect. 4).

We varied the period P of the orbit between 0.1 to 1000 days (dP =0.05 days), and the minimum mass of the companion ($m\,sin[i]$) between 0.1 $M_{\odot}$ to 1000 M_{jup} ($dm\,sin[i]$= 0.05 M_{jup}). We assumed circular orbits, and for each fixed value of the mass and the period we performed 100 simulations randomly chosing the orbital phase between $0 < \phi < 2\pi$. Then we calculated the observed radial velocity of the primary star (RV_{sim}) by means of Equation 9 and, for each simulation, we calculated the dispersion of the radial velocity measurements $\sigma_{obs,sim}$, and the mean radial velocity $\overline{RV_{sim}}$. We finally imposed the conditions that the simulated dispersions and mean radial velocities matched our observed values:

$$\sigma_{obs} - \overline{\sigma_{obs}} \leq \sigma_{obs,sim} \leq \sigma_{obs} + \overline{\sigma_{obs}}, \quad (11)$$

$$|\overline{RV_{obs}} - \overline{RV_{cl}}| - \overline{\sigma_{cl}} \leq |\overline{RV_{sim}} - \overline{RV_{cl}}| \leq |\overline{RV_{obs}} - \overline{RV_{cl}}| + \overline{\sigma_{cl}}, \quad (12)$$

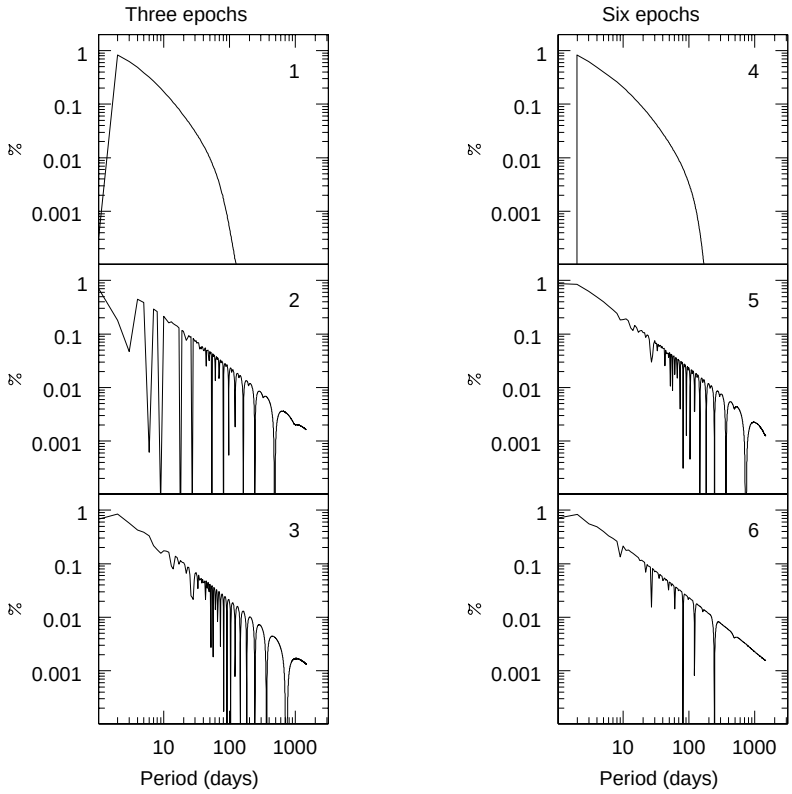

Fig. 13. Probability to detect a planet around a single turn-off star of NGC 6253, in function of the planetary orbital period and different simulated HARPS observing strategies. The left panels show the results considering three observing epochs and the right panels considering six observing epochs, as reported by the labels at the top of each group of panels. Each small panel refers to one of the simulations presented in Table 6, as indicated by the inner numeration.

where $\overline{\sigma_{obs}}$ is our adopted radial velocity error ($\overline{\sigma_{obs}}$ = 0.304 m/s, see Eq. 3). The likelihood a given period and minimum companion mass imply orbits for which the simulated mean radial velocities and dispersions are consistent with our observations, was calculated dividing the number of simulations that matched our criteria, to the total number of simulations. In Fig. 16 (upper panel), we show the likelihood distribution we obtained for star 39810. For periods $P < 3$ days, the mass is m sin(i)$\lesssim$13 M_{jup}, then in the range of massive jupiters. We also plot the theoretical curve (dashed red line) correspondent to $K = 1.4 \times \sigma_{obs}$, which links the observed scatter to the expected radial velocity amplitude of the companion, and the vertical dashed red line indicating a period equal to $\sim 4\times[t3-t1] = 36$ days, which appears to be the maximum period we should expect for the companion object (coincident with a maximum mass equal to m sin(i)=40M_{jup}), at a confidence level $>$ 50%. In Fig. 16 (bottom panel), we show the probability distribution we obtained for the same object, but without the assumption on the barycentric radial velocity of the system (as if the star was a field object). Regions with probability larger than 50% clearly extend toward larger periods and minimum masses ($P > 36$ days, m sin(i) $> 40\ M_{\odot}$).

To better understand this result we performed other simulations, assuming different observing epochs. In Fig. 17, we show the results considering three epochs at $t1 = 486$ days, $t2 = 972$ days, and $t3 = 1458$ days (equally distributed over a period of four years). In both cases (cluster and field star) the overall shape of the probability distribution is the same as in Fig. 16, however the highest probability regions are clearly more extended toward larger masses and periods. The interpretation of Fig. 16 and Fig. 17 is that as long as the period of the companion object is probed by the timescale of the observations (where the timescale can be roughly assumed equal to $4 \times [t3 - t1]$), the most likely mass and period of the companion object producing the observed radial velocity scatter are found along the theoretical curve both for the case of the cluster and of the field star (as traced by the highest probability regions). However, a worse result is obtained for the case of the field star in correspondence of resonant periods. Objects with periods longer than the observing timescale may as well produce a scatter compatible with the observations, but their mass should be larger than what implied by the theoretical curve, since they are forced to produce that scatter during the timescale spanned by the observations. This determines the tail toward large masses and periods visible in Fig. 16. Otherwise, considering the case of the cluster's star, this tail is reduced in extension with respect to the case of the field star, and implies probabilities $<$ 30% thanks to the condition on the barycentric velocity of the system (against $<$ 80% in the case of the field star).

The major conclusion is that if a star belongs to a cluster, and our observations span a period ΔT during which we determine a radial velocity scatter equal to $\sigma_{obs} > \sigma_{cl}$, and a mean radial velocity consistent with the recession velocity of the cluster, the expected mass and period of the suspected companion object are comprised in the region defined by the conditions $K = 1.4\times\sigma_{obs}$, and $P \lesssim 4 \times \Delta T$ in the mass-period diagram, at a confidence

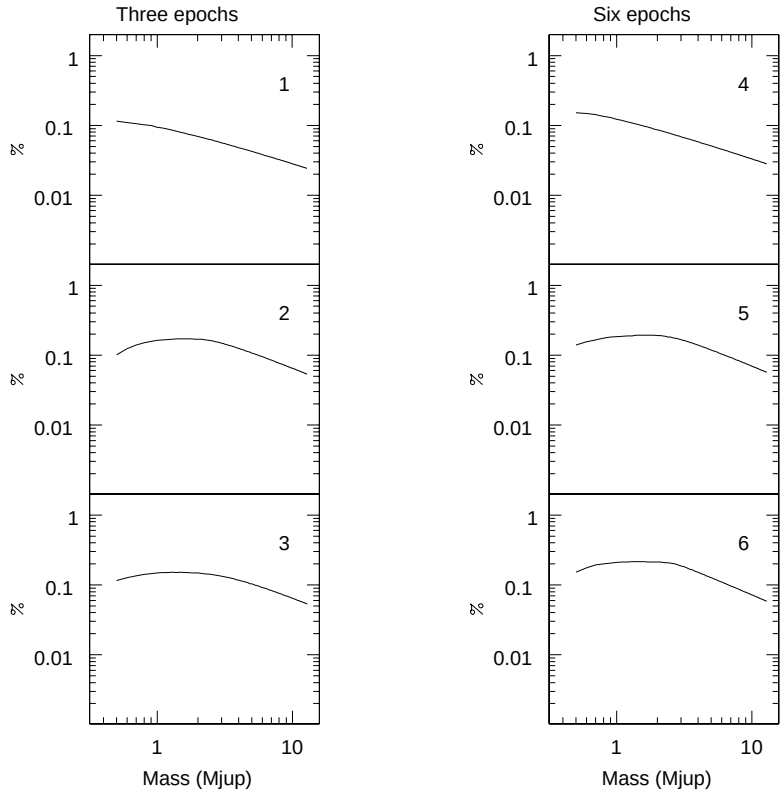

Fig. 14. Same as Fig. 13, but in function of the planetary mass.

level > 50%. This is not true for the case of the field star, where mass and period can be larger than these limits considering the same confidence level.

9.1. The best observing strategy

In Section 8, we derived that three observing epochs equally distributed over a period of four years should provide a good compromize between the number of detectable planets in NGC 6253 and observing time (Table 6). In order to understand how efficient can be this observing strategy to isolate potential planetary candidates, we assumed to observe with the HARPS instrument ($\overline{\sigma_{obs}}$ = 10 m/s), fixing the observing epochs at t1=486, t2=972 and t3=1458 days. We assume to study a star presenting a radial velocity scatter σ_{obs} = 50 m/s. Period and mass of the companion object where varied between 0.05 M_{jup} and 1000 M_{jup}, and between 0.05 days and 1000 days respectively (dP = 0.05 days, $dm\,sin(i)$ = 0.05 M_{jup}). As shown in Fig. 18, the result for the cluster's star resemble more the case of the field star than in previous simulations. The reason is that in this case $\sigma_{obs} << \overline{\sigma_{cl}}$ which reflects the intrinsic dispersion of radial velocities of cluster's stars, then the condition on the mean radial velocity is not as efficient in constraining the period and mass of the orbiting companion as for larger observed σ_{obs} values. Still it is clear that a better result can be obtained than in the case of a field object.

From our survey we have detected five stars having mean radial velocities consistent with the cluster's recession velocity within 0.755 km/s, as shown in Table 7. Moreover they are all cluster's turn-off stars, very likely cluster's members on the basis of our proper motions and radial velocities, and do not present signs of photometric and spectroscopic variability. These objects are: star 40519, 45512, 44104, 45523, and 45267.

Table 7. Turn-off stars of NGC 6253 which are optimal targets for sub-stellar companion searches.

ID_{MO}	$\overline{RV_{obs}} - \overline{RV_{cl}}$ (km/s)
40519	0.063
45512	0.111
44104	0.165
45523	0.277
45267	0.755

Star 39810 discussed above may be instead more properly followed-up using the same UVES/GIRAFFE spectrographs.

We note that also star 45387 has a small radial velocity dispersion, and it is a radial velocity variable, although this object is located in the blue straggler region, and the assumption on the mass of the primary may not be correct. The other close binary systems in our sample are more likley to host stellar companions.

Searching for sub-stellar objects (brown dwarfs and jupiter planets) with the radial velocity technique around old open clusters turn-off stars appears then feasible also with present day instrumentation, but it is necessary: (i) an efficient preselection of candidate cluster's members (by means of colors, magnitudes, and possibly proper motions, and radial velocities); (ii) further identification of massive sub-stellar objects, a task that can be accomplished using multi-object spectrographs like UVES/FLAMES. With just a few hours of observation (6 hours

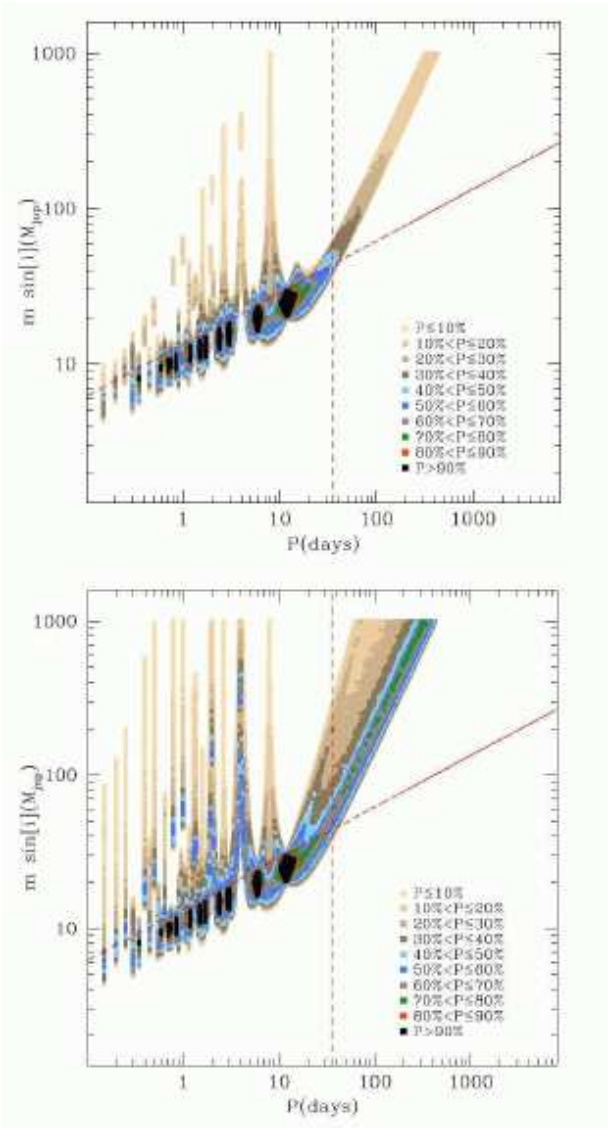

Fig. 16. Period-mass probability distribution for the possible companion object of star 39810, obtained from orbital simulations, assuming the real observing epochs and circular obits. In the upper panel we show the results in the hypothesis that the star belongs to the cluster (as demonstrated by proper motions, radial velocities and position in the CMD), whereas in the bottom panel we show the result if the star was a common field object. σ_{obs} = 1595 m/s, $\overline{\sigma_{obs}}$ = 304 m/s, $\overline{\sigma_{cl}}$ = 850 m/s.

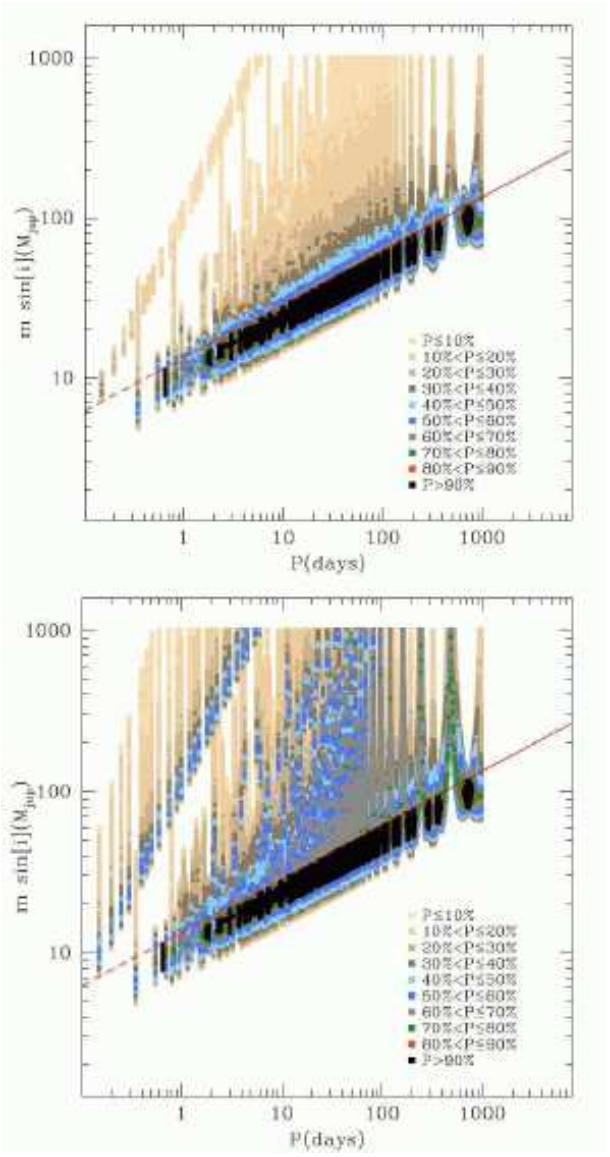

Fig. 17. Same as Fig. 16, assuming three observing epochs at t1=486 days, t2=972 days, and t3=1458 days and circular orbits, σ_{obs} = 1595 m/s, $\overline{\sigma_{obs}}$ = 304 m/s, $\overline{\sigma_{cl}}$ = 850 m/s.

in our case), it is possible to easily cover most of the turn-off members, and identify the best brown dwarf, massive planet candidates, providing at the same time a list of cluster's stars that do not appear radial velocity variables at the precision of these instruments; (iii) this sample, *cleaned* of spurious field contaminants and of large mass-ratio binary systems, can be followed-up with high precision spectroscopy, at first using the same technique of UVES/FLAMES, and then covering more intensively only the most promising targets. The previous steps constitute a sort of roadmap towards detection of sub-stellar objects in open clusters. Proceding by steps, allows to make a more efficient use of observational time.

10. Conclusions

We have presented the results of the first multi-epoch radial velocity survey toward the old metal-rich open cluster NGC 6253. The mean radial velocity of the cluster is $\overline{RV_{cl}} \pm \overline{\sigma_{cl}}$ = (−29.11 ± 0.85) km/s. Using our photometry, proper motions, and radial velocities we identified 35 likely cluster's members, populating the turn-off, sub-giant, red-giant, red clump, and blue straggler regions of the cluster. Among this sample, 12 objects are likely cluster's close binary systems.

We detected one object that may have a companion with a minimum mass in the sub-stellar regime, and that needs to be further investigated: star 39810.

We isolated five turn-off stars that are optimal targets to search for planetary mass companions with the high precision spectroscopy: stars 40519, 45512, 44104, 45523, 45267.

Among the three planetary candidtes we found in the region of NGC 6253, star 171895 is the most interesting objects, requir-

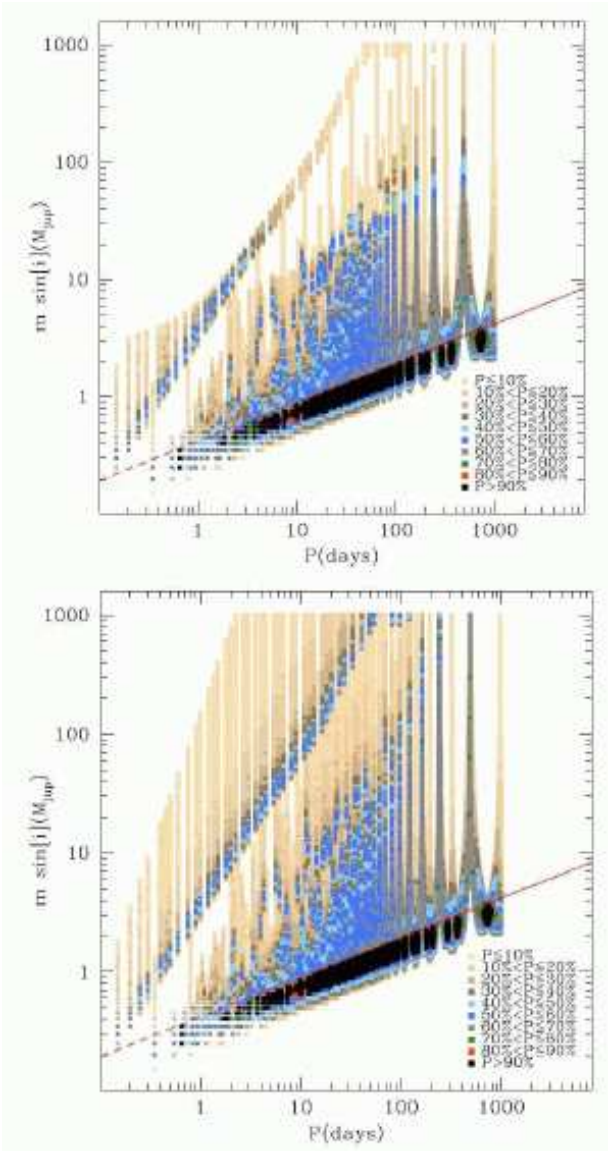

Fig. 18. Same as Fig. 16, assuming three observing epochs at t1=486 days, t2=972 days, and t3=1458 days, circular orbits, σ_{obs} = 50 m/s, $\overline{\sigma_{obs}}$ = 10 m/s, $\overline{\sigma_{cl}}$ = 850 m/s.

ing a more intensive photometric and spectroscopic follow-up in particular with high precision spectroscopy.

We found a new sub-giant branch eclipsing binary system: star 45368.

We compared our results with previous literature radial velocity measurements of a few cluster's members, finding in general a good agreement with our study.

The close binary frequency among turn-off and evolved cluster's stars is f_{cl} =(29±9)% (f_{bin} =[34±10]%, once including also longer period binaries), appears larger than the field binary frequency $f_{cl,field}$ =(22±5)%, although still consistent with that estimate considering the uncertainties.

We showed that searching for sub-stellar objects (brown dwarfs and jupiter planets) with the radial velocity technique around old open clusters turn-off stars, appears feasible also with present day instrumentation, but it is necessary: (i) an efficient pre-selection of candidate cluster's members; (ii) further identification of likely massive sub-stellar objects by means of multi-object spectroscopy; (iii) subsequent follow-up of the best target stars by means of high precision spectroscopy. We derived that three observing epochs uniformly distributed over a period of four years give a good compromise between expected number of detectable planets, and observing time.

In Table 12 we report the cross-correlation among the star's ID introduced in Montalto et al. (2009) and other authours and catalogs.

Very recently Anthony-Twarog et al. (2010) have presented new radial velocity data on NGC 6253 members. These measurements have not been included in our analysis. Merging the results presented in that work with our own results, will allow further identification of the best targets to follow-up more intensively with high resolution spectroscopy to search for sub-stellar companions around cluster's turn-off stars.

Acknowledgements. The authors are grateful to the anonynous referee for the numerous useful comments which have allowed a significant improvement of the paper.

References

Anthony-Twarog, B. J., Twarog, B. A. & Mayer L. 2007, AJ, 133, 1585
Anthony-Twarog, B. J., Deliyannis, C. P.; Twarog, B. A. et al. 2010, AJ, 139, 2034
Ballester, G. E., Modigliani, A., Boitquin, O., et al. 2000, Msngr., 101, 31
Blecha, A., Cayatte, V., North, P., et al. 2000, SPIE, 4008, 467
Bragaglia, A., Tessicini, G., Tosi, M., et al. 1997, MNRAS, 284, 477
Carraro, G., Mendez, R. A., Costa, E. 2005a, MNRAS 356, 647
Carraro, G., Janes, K. A., Eastman, J. D. 2005b, MNRAS 364, 179
Carretta, E., Bragaglia, A., Tosi, M., et al. 2000, ASPC, 198, 273
Carretta, E., Bragaglia, A. & Gratton, R. G. 2007, A&A, 473, 129
Claret 2000, A&A, 363, 1081
Cochran, W. D., Hatzes, A. P., Paulson, D. B. 2002, AJ, 124, 565
De Marchi, F., Poretti, E., Montalto, M., et al. 2009, A&A, accepted
Duquennoy, A. & Mayor, M. 1991, A&A, 248, 485
Endl, M., Cochran, W., D., Küruster, M. et al. 2006, ApJ, 649, 436
Etzel 1981, psbs.conf, 111
Fischer, D. A. & Valenti, J. 2005, ApJ, 622, 1102
Gonzalez, G. 1998, A&A, 334, 221
Hole, K. T., Geller, A. M., Mathieu, R. D., et al. 2009, AJ, 138, 159
Jiang, I.-G., Yeh, L.-C., Chang, Y.-C. et al. 2010, 186, 48
Mermilliod, J.-C., Mayor, M., Udry, S. 2009, A&A, 498, 949
Mandel & Agol 2002, ApJ, 580, 171
Ribas, I. & Miralda-Escudé 2007, A&A, 464, 779
Montalto, M., Piotto G., Desidera, S., et al. 2007, A&A, 470, 1137
Montalto, M., Piotto G., Desidera, S., et al. 2009, A&A, 505, 1129
Pasquini, L., Avila, G., Blecha, A. et al. 2002, Msngr, 110, 1
Piatti, A. E., Clariá, J. J., Bica, E., et al. 1998, AJ, 116, 801
Popper & Etzel 1981, AJ, 86, 102
Sagar, R., Munari, U., & de Boer, K. S. 2001, MNRAS, 327, 23
Santos, N. C., Israelian, G., Mayor, M. 2001, A&A, 373, 1019
Sato, B., Izumiura, H., Toyota, E. et al. 2007, ApJ, 661, 527
Sestito, P., Randich, S. & Bragaglia, A. 2007, A&A, 465, 185
Southworth et al. 2004a, MNRAS, 351, 1277
Southworth et al. 2004b, MNRAS, 355, 986
Southworth, J., & Clausen, J. V. 2006, Ap&SS, 304, 199
Sato, B., Izumiura, H., Toyota, E., et al. 2007, ApJ, 661, 527
Sommariva, V., Piotto, G., Rejkuba, M., et al. 2009, A&A, 493, 947
Tosi, M. 1996, in Leitherer, C., Fritze-von-Alvensleben, U., Huchra, J., eds, ASP Conf. Ser. Vol. 98, The Impact of Stellar Physics on Galaxy Evolution. Astron. Soc. Pac., San Francisco, p. 299
Twarog, B. R., Anthony-Twarog, B. J., & De Lee, N. 2003, AJ, 125, 1383
Wielen R. 1971, A&A, 13, 309

Table 8. ID cross correlation table.

ID_{MO}	ID_{DM}	ID_{BR}	Spectr. Ref.
39621	21000_2	878	
39866	21303_2	1704	
39994	21462_2	2131	
40010	21487_2	2238	
44079	26902_2	904	
44104	26943_2	1393	
44714	28028_2	1027	
45144	28976_2	4181	
45267	29299_2	917	
45285	29358_2	3699	
45300	29398_2	7207	
45368	29635_2	2242	
45387	29695_2	1646	
45403	29716_2	2696	
45404	29718_2	3138	Sestito et al. (2007)
45412	29743_2	2509	Carretta et al. (2007)
45413	29744_2	2508	Carretta et al. (2007)
45421	29754_2	2542	Sestito et al. (2007)
45422	29755_2	2343	
45453	29789_2	1830	
45474	29811_2	2225	Sestito et al. (2007)
45495	29833_2	4227	
45497	29835_2	2400	
45512	29851_2	4391	
45513	29852_2	2864	
45523	29863_2	301	
45524	29864_2	4308	
45528	29868_2	2814	
39810	21234_2	1562	
40519	22119_2	4029	
45414	29745_2	4510	Carretta et al. (2007)
45444	29779_2	2126	
44682	27978_2	307	
45447	29782_2	2726	
45410	29279_2	2885	Carretta et al. (2007)
30341	9268_2	3272	
31195	10340_2	3955	
173273	11351_8	-	
9832	13461_1	7832	
-	15343_2	7502	
24487	1866_2	7006	
38138	19192_2	-	
134894	20096_6	-	
40819	22477_2	4987	
163536	23116_7	-	
-	23129_7	-	
-	23130_7	-	
163548	23133_7	-	
-	23134_7	-	
163549	23135_7	-	
163551	23139_7	-	
163552	23141_7	-	
163560	23150_7	-	
163574	23166_7	-	
163577	23169_7	-	
163588	23181_7	-	
163594	23187_7	-	

Table 8. - continued.

ID_{MO}	ID_{DM}	ID_{BR}	Spectr. Ref.
16649	23368_1	7592	
-	25450_2	3332	
67886	26321_3	-	
67921	26378_3	-	
67922	26379_3	-	
67924	26381_3	-	
-	26383_3	-	
-	26384_3	-	
67926	26387_3	-	
67927	26388_3	-	
67928	26389_3	-	
67929	26391_3	-	
67930	26392_3	-	
67932	26394_3	-	
67934	26396_3	7062	
67936	26399_3	-	
67941	26404_3	-	
67945	26408_3	-	
67946	26409_3	-	
67947	26410_3	-	
67955	26418_3	-	
67966	26429_3	-	
67967	26430_3	-	
67977	26440_3	-	
67985	26448_3	-	
67990	26453_3	-	
68015	26480_3	-	
140621	28393_6	-	
-	28459_6	-	
140634	28460_6	-	
140638	28464_6	-	
140644	28473_6	-	
140646	28475_6	-	
140649	28478_6	-	
140657	28486_6	-	
140669	28498_6	-	
140673	28503_6	-	
140699	28529_6	-	
-	28690_8	-	
-	28694_8	-	
185675	28704_8	-	
185677	28706_8	-	
185680	28709_8	-	
185688	28717_8	-	
185691	28720_8	-	
-	28735_8	-	
185713	28743_8	-	
185716	28746_8	-	
185725	28755_8	-	
45392	29703_2	890	
45396	29707_2	-	
45409	29738_2	5201	
45427	29761_2	-	
45433	29768_2	7049	
45436	29771_2	1222	
-	29788_2	1444	

Table 2 - Proper motion cluster's member stars[9].

ID	ID_{old}	RA(J2000)	DEC(J2000)	V	R	$B-R$	$\overline{RV}$ (km/s)	σ_{obs} (km/s)	$\sigma_{obs}/\overline{\sigma_{obs}}$	MP (%)	class	bin	Inst	D (arcmin)	N
39621	21000_2	254.741554277	-52.739352634	14.986	14.434	1.562	-28.970	0.218	0.719	93	SGB	0	G	2.559	6
39866	21303_2	254.759004492	-52.722501754	14.885	14.342	1.509	-28.846	0.304	1.012	96	SGB	0	G	1.107	3
39994	21462_2	254.716454606	-52.713916592	14.668	14.237	1.244	-32.471	0.272	0.915	92	MS	0	G	3.281	3
40010	21487_2	254.758381195	-52.712023446	14.940	14.378	1.572	-29.059	0.227	0.753	96	SGB	0	G	0.779	3
44079	26902_2	254.760879590	-52.738914968	15.081	14.613	1.311	-6.142	35.258	100.587	90	RSCVn	1	G	1.929	6
44104	26943_2	254.719145710	-52.728702583	14.674	14.245	1.244	-29.275	0.268	0.901	97	MS	0	G	3.333	6
44714	28028_2	254.771428094	-52.736500368	14.767	14.355	1.198	-32.104	0.303	1.008	95	MS	0	G	1.690	3
45144	28976_2	254.711383740	-52.672184921	14.689	14.272	1.221	-34.989	5.081	17.041	97	MS	1	G	4.175	6
45267	29299_2	254.782265985	-52.738724213	14.566	14.126	1.263	-29.865	0.221	0.752	97	MS	0	G	1.948	3
45285	29358_2	254.812305421	-52.682399611	14.596	14.174	1.221	-32.232	0.286	0.969	97	MS	0	G	2.935	6
45300	29398_2	254.820509709	-52.633893784	14.913	14.268	1.793	24.414	0.256	0.859	94	RGB	0	G	5.371	6
45368	29635_2	254.821529886	-52.712167009	14.775	14.344	1.558	-2.927	109.131	363.382	95	RGB(EA)	1	G	3.052	3
45387	29695_2	254.777712300	-52.723913985	13.588	13.336	0.803	-29.602	1.602	5.932	97	BSS	1	G	1.022	3
45403	29716_2	254.738719335	-52.702446444	14.408	13.975	1.235	-7.056	39.078	135.101	97	MS	1	G	1.958	3
45404	29718_2	254.803860426	-52.693301033	13.501	1.793	12.852	-30.384	0.281	1.100	97	RGB	0	G	2.178	6
45412	29743_2	254.816478798	-52.707251010	12.664	1.946	11.977	-28.323	0.280	1.221	93	RC	0	G	2.740	3
45413	29744_2	254.766037019	-52.707003744	12.666	1.927	11.980	-32.877	0.259	1.129	91	RC	0	G	0.299	6
45421	29754_2	254.779357160	-52.706134064	13.175	1.976	12.468	-18.380	0.339	1.389	94	RGB	0	G	0.529	6
45422	29755_2	254.771091308	-52.710302821	12.663	12.473	0.645	-26.335	0.512	2.097	93	BSS	0	G	0.119	6
45453	29789_2	254.829986625	-52.720451714	14.093	13.430	1.850	-22.830	0.341	1.250	97	RGB	0	G	3.623	3
45474	29811_2	254.721883313	-52.712070185	14.275	1.252	13.842	-21.816	8.090	28.360	96	MS	1	G	2.946	3
45495	29833_2	254.819240417	-52.671697278	14.581	14.013	1.610	-28.465	0.313	1.078	97	SGB	0	G	3.643	6
45497	29835_2	254.784723840	-52.709401070	14.230	14.015	0.717	-21.231	0.824	2.837	94	BSS	0	G	0.836	3
45512	29851_2	254.827234336	-52.667990504	14.526	14.089	1.268	-29.221	0.214	0.731	96	MS	0	G	4.161	6
45513	29852_2	254.767975414	-52.698951512	14.579	14.089	1.396	-32.957	0.375	1.281	92	SGB	0	G	0.589	3
45523	29863_2	254.769166510	-52.752381830	14.579	14.148	1.247	-29.387	0.290	0.985	97	MS	0	G	2.645	3
45524	29864_2	254.786506052	-52.669549018	14.634	14.154	1.379	-27.708	0.360	1.222	96	SGB	0	G	2.510	3
45528	29868_2	254.776058961	-52.700222056	14.603	14.182	1.225	-91.691	20.931	70.842	97	MS	1	G	0.579	3
39810	21234_2	254.798041667	-52.725666667	14.939	14.475	1.319	-29.269	1.595	5.242	95	MS	1	U	1.936	3
40519	22119_2	254.677458333	-52.674722222	14.730	14.307	1.220	-29.047	0.157	0.525	97	MS	0	U	5.953	3
45414	29745_2	254.775458333	-52.665472222	12.713	1.981	12.000	-27.398	0.145	0.630	91	RC	0	U	2.587	3
45444	29779_2	254.753875000	-52.714277778	13.516	13.221	0.937	-31.131	0.093	0.349	95	BSS	0	U	1.078	3
44682	27978_2	254.751808989	-52.752259663	14.850	14.406	1.277	-40.929	0.326	1.079	95	MS	0	U	2.871	3
45447	29782_2	254.786291667	-52.702111111	13.575	13.276	0.928	-28.337	0.335	1.249	97	BSS	0	U	1.000	3
45410	29279_2	254.751791667	-52.752250000	12.629	11.896	2.022	-28.366	0.241	1.062	91	RC	0	U	2.871	3
30341	9268_2	254.720919972	-52.690243537	16.244	15.592	1.811	13.915	1.277	1.734	87	EW	0	G	3.185	6

[9] Star 30341 is a very likely field star sharing the same proper motion of cluster's members, as discussed in Sect. 4. The R band magnitude for star 45410 is taken from Bragaglia et al. (2007).

Table 3 - Proper motion non members or stars with doubtful/undefined proper motions.

ID	ID_{old}	RA(J2000)	DEC(J2000)	V	R	$B-R$	$\overline{RV}$ (km/s)	σ_{obs} (km/s)	$\sigma_{obs}/\overline{\sigma_{obs}}$	PM (%)	class	bin	Inst	D (arcmin)	N
31195	10340_2	254.706854237	-52.676396811	16.397	15.898	1.419	-32.657	0.362	0.422	38	EA	0	G	4.291	6
173273	11351_8	254.896720660	-52.836752470	15.205	14.465	2.025	-42.661	30.105	99.046	-	LON	1	G	10.790	3
9832	13461_1	254.962830875	-52.606220233	15.459	15.034	1.216	-2.792	0.630	1.220	-	RO1	0	G	13.047	3
-	15343_2	254.770702368	-52.609720836	15.863	15.370	-	-67.992	0.623	0.960	-	LON	0	G	5.917	6
24487	1866_2	254.653965066	-52.793810375	16.343	15.854	1.342	-75.686	92.910	110.676	0	EA	1	G	8.687	6
38138	19192_2	254.706610743	-52.557441173	16.732	16.338	1.138	18.848	0.083	0.081	-	EA	0	G	9.840	3
134894	20096_6	254.417758709	-52.895986437	14.252	13.864	1.088	-28.813	19.067	66.686	-	FLD	1	G	23.991	3
40819	22477_2	254.690203633	-52.656152556	15.708	15.014	1.908	-52.738	36.375	71.532	3	LON	1	G	5.763	6
163536	23116_7	254.722213314	-52.948895073	13.415	13.046	0.932	7.981	57.000	218.073	-	FLD	1	G	14.726	6
-	23129_7	254.799930441	-52.887540489	11.520	10.496	-	-54.056	0.242	1.309	-	FLD	0	G	10.893	3
-	23130_7	254.757225314	-52.877753023	12.086	11.024	-	-103.293	0.053	0.264	-	FLD	0	G	10.198	3
163548	23133_7	254.669827025	-52.930392670	12.211	11.767	1.150	19.665	0.269	1.206	-	FLD	0	G	14.637	6
-	23134_7	254.803057832	-52.882388381	12.725	11.939	-	-28.732	0.313	1.372	-	FLD	0	G	10.621	3
163549	23135_7	254.689049938	-52.897896575	12.179	11.998	0.466	69.037	12.904	56.119	-	FLD	1	G	12.387	3
163551	23139_7	254.798903713	-52.953877042	13.138	12.282	2.225	-167.759	0.322	1.350	-	FLD	0	G	14.828	3
163552	23141_7	254.706644063	-52.935814623	12.811	12.371	1.145	14.942	0.277	1.149	-	FLD	0	G	14.182	6
163560	23150_7	254.724173431	-52.959861120	13.211	12.894	0.812	-32.828	0.656	2.554	-	FLD	0	G	15.349	3
163574	23166_7	254.669018969	-52.950165598	14.014	13.398	1.563	-11.943	0.064	0.235	-	FLD	0	G	15.743	3
163577	23169_7	254.670152457	-52.892319670	13.898	13.445	1.162	-9.687	0.352	1.288	-	FLD	0	G	12.583	6
163588	23181_7	254.858525155	-52.826803097	14.072	13.689	0.984	6.743	1.463	5.213	-	FLD	1	G	8.844	3
163594	23187_7	254.684863939	-52.908620251	14.209	13.796	1.087	-12.892	0.667	2.350	-	FLD	0	G	13.077	3
16649	23368_1	254.892499238	-52.618200382	16.040	15.549	1.347	-28.046	4.725	6.569	-	LON	1	G	9.086	6
-	25450_2	254.805044466	-52.689669137	14.998	14.414	-	-33.368	0.119	0.393	-	SGB	0	G	2.339	3
67886	26321_3	254.482589823	-52.662323933	14.312	14.142	0.544	114.585	0.402	1.366	-	FLD	0	G	17.513	3
67921	26378_3	254.413264184	-52.633466144	11.750	11.143	1.638	-7.640	0.068	0.333	-	FLD	0	G	21.920	3
67922	26379_3	254.578046170	-52.648945160	11.671	11.258	1.090	-10.953	0.155	0.746	-	FLD	0	G	12.103	3
67924	26381_3	254.543038176	-52.787773870	12.385	11.709	1.840	-49.386	0.102	0.461	-	FLD	0	G	14.474	3
-	26383_3	254.495800014	-52.654929150	12.126	11.857	-	0.273	2.660	11.785	-	FLD	1	G	16.811	3
-	26384_3	254.467238532	-52.678488517	12.706	11.979	-	-29.002	0.237	1.033	-	FLD	0	G	18.303	3
67926	26387_3	254.539435308	-52.696231477	12.589	12.136	1.269	34.571	0.053	0.226	-	FLD	0	G	13.903	3
67927	26388_3	254.563036304	-52.700631570	13.250	12.295	2.466	-45.090	0.222	0.929	-	FLD	0	G	12.476	6
67928	26389_3	254.622359288	-52.788928390	13.271	12.340	2.459	-129.620	0.064	0.266	-	FLD	0	G	10.135	3
67929	26391_3	254.549734704	-52.697411770	13.260	12.360	2.376	-19.561	0.228	0.947	-	FLD	0	G	13.282	6
67930	26392_3	254.567889707	-52.652336950	12.963	12.400	1.418	-10.743	0.234	0.967	-	FLD	0	G	12.632	3
67932	26394_3	254.561569146	-52.777658932	13.164	12.429	1.974	33.301	0.021	0.086	-	FLD	0	G	13.226	3
67934	26396_3	254.608100708	-52.746645350	13.263	12.453	2.170	-64.018	0.398	1.634	-	FLD	0	G	10.030	6

Table 3 - continued.

ID	ID_{old}	RA(J2000)	DEC(J2000)	V	R	$B-R$	$\overline{RV}$ (km/s)	σ_{obs} (km/s)	$\sigma_{obs}/\overline{\sigma_{obs}}$	PM (%)	class	bin	Inst	D (arcmin)	N
67936	26399_3	254.626618858	-52.787154573	12.902	12.544	0.983	18.784	0.206	0.836	-	FLD	0	G	9.860	3
67941	26404_3	254.442086101	-52.607335252	13.367	12.633	1.991	-113.170	0.050	0.201	-	FLD	0	G	20.636	3
67945	26408_3	254.585780949	-52.586474088	13.265	12.794	1.298	-9.438	0.135	0.532	-	FLD	0	G	13.294	3
67946	26409_3	254.512752456	-52.613015638	13.573	12.803	2.044	23.039	0.120	0.472	-	FLD	0	G	16.508	3
67947	26410_3	254.477436426	-52.709457932	13.220	12.859	1.043	-3.022	0.064	0.250	-	FLD	0	G	17.604	3
67955	26418_3	254.565924874	-52.651266667	13.782	13.076	1.897	-28.716	0.130	0.496	-	FLD	0	G	12.763	3
67966	26429_3	254.449296536	-52.638328004	13.735	13.320	1.065	-58.091	0.057	0.211	-	FLD	0	G	19.745	3
67967	26430_3	254.476022606	-52.610630605	13.680	13.328	0.960	-8.980	0.216	0.800	-	FLD	0	G	18.635	3
67977	26440_3	254.530417244	-52.694176623	13.821	13.515	0.889	-27.161	11.016	39.993	-	FLD	1	G	14.450	6
67985	26448_3	254.545224278	-52.819864168	14.039	13.654	1.067	-21.709	0.432	1.545	-	FLD	0	G	15.101	3
67990	26453_3	254.511619302	-52.592918131	14.195	13.772	1.169	59.842	0.069	0.244	-	FLD	0	G	17.024	3
68015	26480_3	254.497327009	-52.592069063	14.423	14.168	0.765	-40.474	0.158	0.536	-	FLD	0	G	17.832	3
140621	28393_6	254.548942740	-52.882868333	14.315	13.950	1.022	-38.038	0.133	0.461	-	FLD	0	G	16.939	3
-	28459_6	254.499009772	-52.929900629	12.129	11.092	-	-109.233	0.108	0.533	-	FLD	0	G	21.041	3
140634	28460_6	254.507839490	-52.848165436	12.123	11.515	1.710	1.368	0.294	1.365	-	FLD	0	G	17.871	3
140638	28464_6	254.570293491	-52.938044259	12.485	11.747	2.063	-37.547	0.148	0.665	-	FLD	0	G	18.295	3
140644	28473_6	254.504500607	-52.942293210	13.191	12.383	2.231	12.192	0.190	0.787	-	FLD	0	G	21.270	3
140646	28475_6	254.456714683	-52.923391210	12.785	12.440	0.947	-24.579	0.570	2.344	-	FLD	0	G	22.841	3
140649	28478_6	254.544458763	-52.865185343	12.806	12.497	0.900	-30.448	0.206	0.841	-	FLD	0	G	16.524	3
140657	28486_6	254.429351125	-52.875500987	13.156	12.833	0.931	-18.260	0.335	1.314	-	FLD	0	G	22.812	3
140669	28498_6	254.616850167	-52.859586692	13.632	13.188	1.210	-45.815	0.333	1.254	-	FLD	0	G	12.951	3
140673	28503_6	254.450929209	-52.875536659	13.665	13.247	1.143	-10.783	0.275	1.028	-	FLD	0	G	21.658	3
140699	28529_6	254.543259382	-52.943814112	14.080	13.712	1.012	-44.742	1.899	6.749	-	FLD	1	G	19.648	3
-	28690_8	254.939726170	-52.841313814	11.932	10.995	-	29.589	0.352	1.761	-	FLD	0	G	12.897	3
-	28694_8	254.889275229	-52.937219928	12.712	11.677	-	-14.678	0.407	1.847	-	FLD	0	G	15.463	3
185675	28704_8	255.024101352	-52.918452706	13.354	12.406	2.287	-45.233	0.320	1.321	-	FLD	0	G	19.745	3
185677	28706_8	254.994626725	-52.932280496	13.282	12.488	2.112	-41.967	0.308	1.259	-	FLD	0	G	18.995	3
185680	28709_8	254.926017918	-52.900682171	13.354	12.550	2.109	-29.071	0.367	1.489	-	FLD	0	G	14.829	3
185688	28717_8	254.904752739	-52.936850862	13.518	12.847	1.769	2.067	0.232	0.908	-	FLD	0	G	15.892	3
185691	28720_8	254.990056545	-52.881001312	13.359	13.007	0.950	29.770	0.126	0.484	-	FLD	0	G	16.743	3
-	28735_8	254.989955098	-52.890883421	13.757	13.303	-	-86.628	1.654	6.147	-	FLD	1	G	17.112	3
185713	28743_8	255.019022079	-52.870890883	13.950	13.526	1.145	50.173	0.533	1.933	-	FLD	0	G	17.801	3
185716	28746_8	254.942219159	-52.864234008	14.031	13.604	1.141	-66.787	0.259	0.931	-	FLD	0	G	13.901	3
185725	28755_8	255.023227456	-52.880776292	14.114	13.750	1.003	-16.067	0.361	1.278	-	FLD	0	G	18.341	3
45392	29703_2	254.824144074	-52.739573624	13.780	13.460	0.942	-28.956	0.220	0.804	69	BSS	0	G	3.708	6
45396	29707_2	254.689317405	-52.575108639	13.289	12.908	1.162	-35.859	0.030	0.117	33	BSS	0	G	9.371	3

Table 3. [10] **- continued.**

ID	ID_{old}	RA(J2000)	DEC(J2000)	V	R	$B-R$	$\overline{RV}$ (km/s)	σ_{obs} (km/s)	$\sigma_{obs}/\overline{\sigma_{obs}}$	PM (%)	class	bin	Inst	D (arcmin)	N
45409	29738_2	254.839975270	-52.726039925	12.148	11.890	0.750	-23.235	1.473	6.498	85	BSS	1	G	4.283	6
45427	29761_2	254.708887513	-52.576116956	13.003	12.641	1.079	-29.748	0.549	2.203	58	BSS	0	G	8.761	3
45433	29768_2	254.839119879	-52.606605106	13.038	12.929	0.484	-32.196	0.545	2.113	65	BSS	0	G	7.353	6
45436	29771_2	254.830276966	-52.732927498	13.247	12.984	0.806	-13.477	0.585	2.254	1	BSS	0	G	3.860	3
-	29788_2	254.791380060	-52.727963547	14.301	13.419	-	-43.524	16.173	59.335	-	RGB	1	G	1.705	3
45464	29801_2	254.651225693	-52.675666413	13.955	13.641	0.928	9.764	0.343	1.228	61	BSS	0	G	7.439	6
71299	30211_3	254.461672728	-52.706299798	11.120	-	-	-38.034	21.938	116.320	-	FLD	1	G	18.550	3
21536	31067_1	254.966090567	-52.719334972	12.717	12.538	0.591	15.639	2.244	9.117	-	FLD	1	G	11.734	3
-	31087_1	254.989667455	-52.697548585	11.327	10.324	-	-48.930	0.373	2.075	-	FLD	0	G	13.146	3
-	31090_1	255.007768469	-52.668891270	11.750	11.097	-	-17.765	0.436	2.149	-	FLD	0	G	14.413	3
21554	31099_1	254.896158044	-52.773508224	12.745	12.198	1.589	-31.313	0.242	1.026	-	FLD	0	G	8.476	3
21555	31100_1	254.890108159	-52.669401644	12.854	12.206	1.784	-32.129	0.055	0.233	-	FLD	0	G	7.529	3
21558	31103_1	254.916049117	-52.817951093	12.991	12.240	2.073	-28.603	0.357	1.505	-	FLD	0	G	10.917	3
21561	31106_1	255.003618185	-52.722222163	13.093	12.332	2.131	-19.685	0.397	1.654	-	FLD	0	G	13.993	3
21563	31108_1	254.934329679	-52.690130737	13.062	12.349	1.996	-7.988	0.442	1.838	-	FLD	0	G	9.871	3
21570	31117_1	254.943244134	-52.794388447	13.379	12.581	2.190	5.329	0.276	1.115	-	FLD	0	G	11.562	6
21575	31122_1	254.906583525	-52.811952487	13.132	12.744	1.144	-8.498	0.055	0.218	-	FLD	0	G	10.246	3
21579	31127_1	254.934399254	-52.787946227	13.215	12.907	0.949	19.976	0.096	0.373	-	FLD	0	G	10.915	3
21586	31134_1	254.916294437	-52.624260203	13.709	13.210	1.400	25.242	0.292	1.097	-	FLD	0	G	10.080	3
21595	31143_1	255.003967260	-52.808132026	13.674	13.373	0.938	-26.024	0.249	0.918	-	FLD	0	G	15.216	3
21596	31144_1	255.071319344	-52.670928513	13.874	13.412	1.299	-11.124	0.292	1.072	-	FLD	0	G	18.170	3
187962	31292_8	254.910829697	-52.859514420	11.736	-	-	-7.293	0.306	1.478	-	FLD	0	G	12.362	3
-	32759_1	255.049177249	-52.694093487	11.634	-	-	31.759	0.159	0.779	-	FLD	0	G	16.723	3
74452	4180_4	254.326743597	-52.796666245	15.283	15.053	0.771	-66.219	0.858	1.638	-	RR	0	G	27.167	3
50025	5668_3	254.623806426	-52.661485581	15.796	15.138	1.756	-71.127	8.200	14.712	-	LON	1	G	9.258	3
4306	5891_1	255.080076806	-52.726794719	15.633	14.989	1.613	-0.495	43.463	87.159	-	LON	1	G	18.588	3
-	8420_6	254.504434833	-52.893020827	14.657	14.413	-	-98.949	9.747	32.233	-	DSCT	1	G	19.449	3
126376	8541_6	254.518259628	-52.889120371	14.919	14.447	1.282	-6.395	0.107	0.353	-	EA	0	G	18.637	6
6430	8864_1	255.028469607	-52.679450408	16.056	15.540	1.402	-10.028	59.256	82.788	-	RO2	1	G	15.556	3
171895	9471_8	254.964382916	-52.896065953	15.260	14.738	1.367	-51.810	0.233	0.583	-	TRS	0	U	16.178	3
23333	434_2	254.787757895	-52.814363476	18.247	17.634	1.662	-13.602	1.565	1.016	-	TRS	0	U	6.442	6

[10] (Col.1) ID of Montalto et al. (2009). (Col.2) ID of De Marchi et al. (2009). (Col. 3) Right ascension in degrees. (Col.4) Declination of the star in degrees. (Col. 5) V magnitude. (Col.6) R magnitude. (Col.7) $B-R$ color in the seventh column. (Col.8) Mean radial velocity of the star (RV_{obs}). (Col.9) Dispersion of the radial velocity measurements (σ_{obs}). (Col.10) the value of $\sigma_{obs}/\overline{\sigma_{obs}}$. (Col.11) proper motion membership probability (MP). (Col.12) Classification code: MS (=main sequence), SGB (=sub-giant branch), RGB (=red-giant branch), RC (=red clump), BSS (=blue straggler), RSCVn (=RS Canum Venaticorum variable), EW (=contact binary), EA (=Algol variable, detached system), LON (=Long period variable >10 days), RO1, RO2 (=rotational variables, see De Marchi et al. 2009 for details), RR (=RR Lyrae), DSCT (=δ Scuti), TRS (=transiting planetary candidate). (Col.13) the binarity index (equal to 1 if, on the basis only of our own radial velocities, the star is considered a binary, 0 if it is considered a single star). (Col.14) Spectrograph used to study the star, either UVES (U), or GIRAFFE (G). (Col.15) The projected radial distance from the cluster's center in arcmin. (Col.16) The number (N) of measurements obtained.

Table 8. - continued[11].

ID_{MO}	ID_{DM}	ID_{BR}	Spectr. Ref.
45464	29801_2	7096	
71299	30211_3	-	
21536	31067_1	-	
-	31087_1	-	
-	31090_1	-	
21554	31099_1	7041	
21555	31100_1	7045	
21558	31103_1	-	
21561	31106_1	7053	
21563	31108_1	7052	
21570	31117_1	7068	
21575	31122_1	7055	
21579	31127_1	7063	
21586	31134_1	7084	
21595	31143_1	-	
21596	31144_1	-	
187962	31292_8	-	
-	32759_1	-	
74452	4180_4	-	
50025	5668_3	7478	
4306	5891_1	-	
-	8420_6	-	
126376	8541_6	-	
6430	8864_1	-	
171895	9471_8	-	
23333	434_2	9836	

[11]In Col. 1 we report the numeration of Montalto et al. (2009), in Col. 2 the numeration of De Marchi et al. (2009), in Col. 3 the numeration of the WEBDA. In Col. 4 the reference for those stars that were already spectroscopically studied by other authors.